Senior Thesis

Experiment to Test Ground Penetrating Radar for Gasoline Detection

by

Jeffrey T. McAllister

1994

Submitted as partial fulfillment of
the requirements for the degree of
Bachelor of Science in Geology and
Mineralogy at The Ohio State University,
Summer Quarter, 1994.

Approved by:

Dr. Jeffrey J. Daniels

Dedicated to the memory of

* James A. Apple *

I could not have asked for a better Uncle.

Acknowledgements

My sincere appreciation is expressed to Dr. Jeffrey J. Daniels for his guidance, support, and direction throughout the course of this study. I especially thank him for his interest and dedication to research and education.

I wish to express my gratitude to Mr. David Grumman, who assisted and guided me through the various fundamentals of GPR and the processing techniques.

I also wish to thank all those individuals who contributed to the development and completion of this thesis, especially Mr. Kurt Hayden, Mr. Jens Munk, and Mr. Roger Roberts.

Special thanks to the U.S. EPA, Region V for use of the 500Mhz antenna and to Geophysical Survey Systems, Inc. for the use of the 900Mhz antenna and the SIR System 10.

My utmost appreciation goes to my parents who supported, encouraged, and never gave up on me during any of my endeavors through college or in life.

To my wife, thanks for everything!

Abstract

Ground Penetrating Radar (GPR) is a shallow, noninvasive, geophysical survey technique. It has been used in the past for detection and mapping of Light Non-Aqueous Phase Liquids (i.e., Hydrocarbons). With the increasing contamination of ground water supplies by substances such as hydrocarbons, an inexpensive, reliable, and simple geophysical technique such as GPR is a must. Although the scientific community knows that GPR works, they do not know exactly what contamination zone (i.e., gasoline saturation, vapor, etc...) the GPR system actually detects. It is also unknown exactly how these different gasoline zones effect the velocity of the GPR waves. This thesis presents an overview of 1) the fundamentals of GPR, 2) geologic applications, 3) subsurface contaminants, and 4) detection of contaminants in the field. These sections will be followed by an experiment that tests the ability of GPR to detect gasoline in a perfectly homogenous medium.

GPR Background

Ground penetrating radar (GPR) has been developed for investigations of subsurface objects that have electrical properties that are in contrast with the surrounding medium. These investigations are shallow (<30m), and high resolution in nature. In the field, GPR can be used to gather a large amount of data

quickly. The mobility of the system and the ease of use in the field makes GPR excellent for geotechnical techniques.

Fundamentals

Ground penetrating radar is similar to a common "graph fish finder" or acoustic sonogram. Electromagnetic waves are produced by a transmitter antenna. Waves are then reflected back to a receiver antenna and recorded. There are two types of antennas 1) bistatic, and 2) monostatic. The components of a GPR system are shown in Figure 1. (Daniels, 1989). A bistatic mode antenna is one in which there is a separate transmitter and receiver. Monostatic mode antennas use the same antenna for both transmitting and receiving waves. Monostatic mode antennas are also the most common type of antennas. The frequency produced by antennas range from 25Mhz to 1Ghz. Since high frequency wavelengths are easily absorbed, high frequency antennas (>200Mhz) are shielded as to direct the signal downward only. Low frequency antennas (<200Mhz) are usually not shielded. Both types of antennas can be moved by hand or by being towed by some type of vehicle, as long as the method of transportation does not effect the GPR signal. The GPR system can collect several line-kilometers of data along profile lines spaced a few meters (or fractions of meters) apart (Daniels, Roberts, 1989). In general, the antennas are identified by its center band frequency, for example, 500Mhz, 900Mhz (Daniels, 1989). High frequency antennas have lower depth penetration and higher resolution. Low frequency antennas have greater depth penetration and lower resolution.

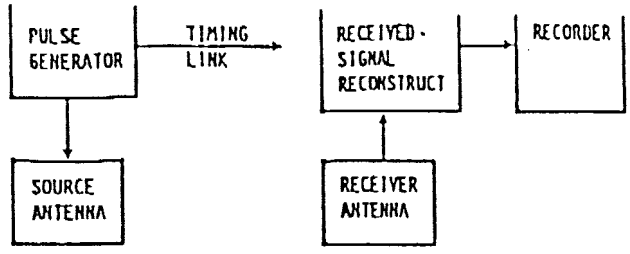

(a) GPR system.

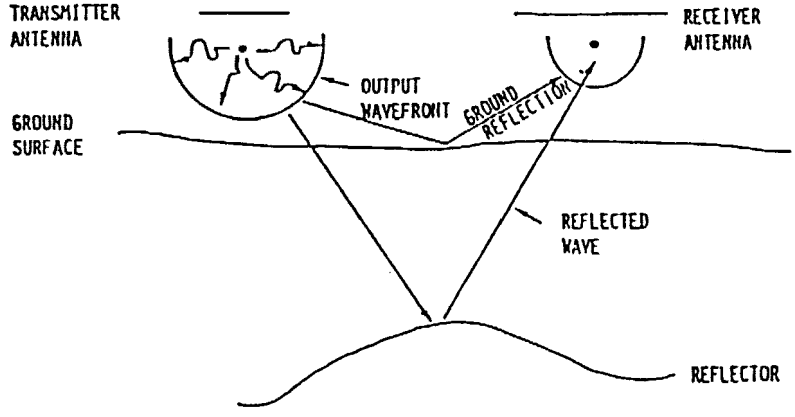

(b) Bistatic mode antenna.

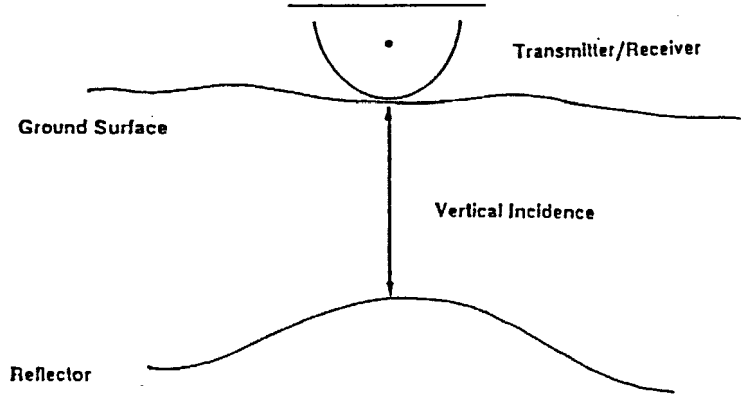

(c) Monostatic mode antenna.

Figure 1. Operating components and modes of GPR. (a) Generalized diagram of GPR components. (b) Bistatic antenna operating mode. (c) Monostatic antenna operating mode.

(Daniels, 1989)

Most GPR systems use a time-domain pulse system, and nearly all of the systems that are used for engineering and environmental applications (including Geo-Centers, GSSI, OYO, and Sensors and Software) utilize a time-domain pulse system (Daniels, 1989). The advantage of this system is that the received pulse can be interpreted immediately with no pre-processing to "clean-up" the records.

The transmitter produces an electromagnetic pulse which travels downward until it comes into contact with an object that has a different electrical impedance than the surrounding medium. Both the transmitted and reflected pulses are then recorded. If the transmitted pulse does not encounter an object of a different electrical impedance, then only the transmitted pulse will be recorded. This distance of wavefront movement is known as the two-way travel time (Figure 2., Daniels, Roberts, 1994). Two-way travel time represents the total time it takes the transmitted and reflected wave to travel through the surrounding medium. This travel time is in the units of nanoseconds (ns), where 1ns = 10^{-9}s. The average total recording time is roughly between 10 to 1000ns. The record of a single transmitted pulse, and the resulting reflections plotted as a function of time and amplitude is called a scan (total recording time) (Figure 3., Daniels, 1989).

A GPR record consists of a series of scans that can be sampled at 2ns intervals, but this can be reduced to smaller intervals using such techniques as ensamble-averaging (Daniels, 1989). Two types of GPR recordings traces/scans are shown in Figure 4 (Daniels, 1989) including: a) wiggle trace display, where the

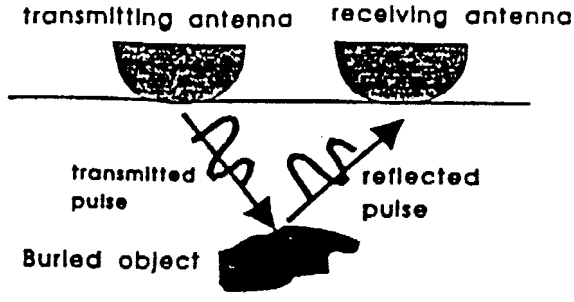

(a) An electromagnetic pulse is transmitted, travels through the ground, is reflected, and travels to the receiver antenna.

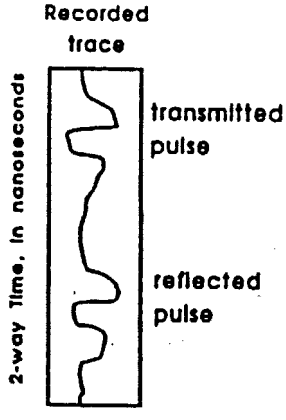

(b) A simple trace from a buried object consists of the transmitted pulse traveling through the air and the reflected pulse.

Figure 2. The making of a single time trace, with transmitter and receiver antennas at a single point on the surface.

(Daniels, Roberts, 1994)

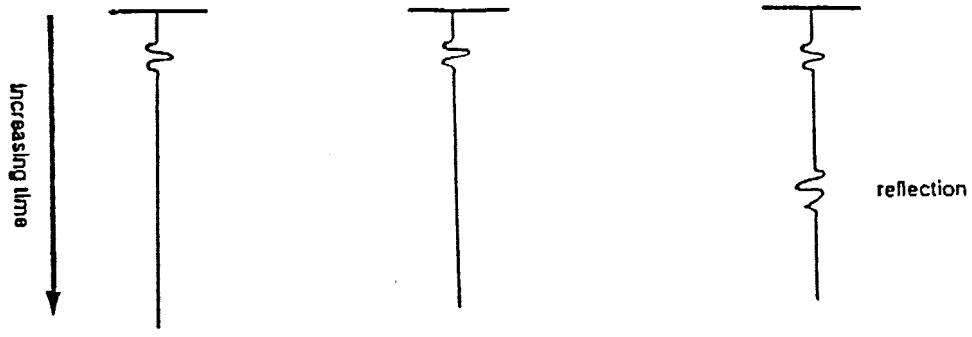

(a) Transmitted pulse. (b) Received scan over halfspace. (c) Received scan over a layer interface.

Figure 3. (a) Transmitted time domain pulse with typical pulse shape. (b) Recorded signal over a homogenous halfspace. (c) Recorded signal over a reflector.

(Daniels, 1989)

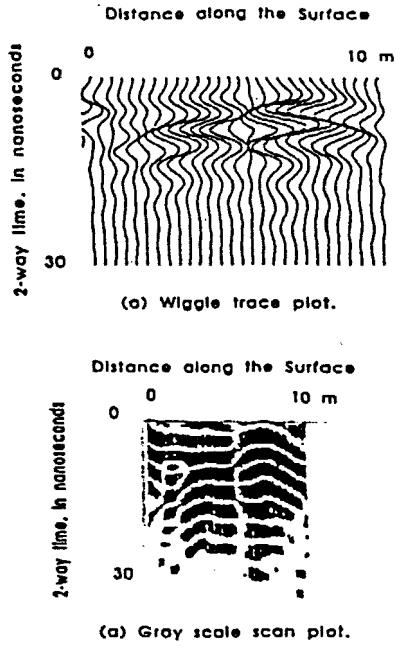

Figure 4. Comparison of wiggle trace and gray scale scan record displays. Anomalies are caused by two buried barrels.

(Daniels, 1989)

intensity of the received wave at an instant of time is proportional to the amplitude of the wiggle, and b) gray-scale display, where the intensity of the received wave at an instant in time is proportional to the intensity of the gray-scale (i.e. black is high intensity, white is low intensity) (Daniels, Roberts, 1994). These types of records can be displayed depending on the operator's own preference. There are several ways of displaying the data, some being color displays and printers.

Detection and Resolution

Many conditions must be met in order for a buried object to be detected by a GPR system:

1) The transmitted wave must be of a sufficient power to reach the buried object and return to the surface to be detected by the receiver.

2) The impedance contrast of the buried body must be high enough to cause a sufficient reflection.

3) The object must be large enough to be detected at the specified depth.

4) Other objects must not interfere with the reflection emanating from the buried object. (Daniels, 1989).

We must remember that some material cannot be penetrated by electromagnetic waves (i.e., soils high in clay content).

Resolution, as stated by Daniels, (1989) is the ability to detect and define a buried target. It is also known as the capability of distinguishing the top and bottom of a second layer in a three layer model. Resolution is dependent on six criteria:

1) the amplitude in wavelength of the transmitted pulse,

2) the electrical properties and electromagnetic propagation characteristics of the host material,

3) the complexity of the geology

4) noise from manmade objects at, or near, the surface,

5) the depth, shape, and size of the target,

6) the electrical impedance of the target. (Daniels, 1989).

There is loss in resolution from things such as depth, multiple reflections, antenna ringing, target resonance, interference from outside sources, and even from shallow geologic layers. In fact, the interference and signal attenuation caused by a shallow target may totally mask any reflection from a deeper target (Daniels, 1989).

GPR in the Field

Not unlike other geophysical survey techniques, with GPR, one has to have an idea of what they are looking for before starting to survey the area. A general list of field procedures that might be used is summarized by Daniels, (1989):

1) Select a test line

2) Select a means of towing the antennas

3) Determine the profile or gridline pattern

4) Calibrate the recorder and electronics

5) Test the available antennas along the test line

6) Run the survey

7) Re-run the test lines

8) Determine the velocity from the target buried at a known depth, or a walk-away test if two antennas are available and the material is layered

9) Measure the near-surface electrical properties with a radio frequency probe (if available). These measurements should be made on the test line, and at other critical locations in the survey area.

Determination of where to run a test line is one of the most important decisions that has to be made. The test line should not be located anywhere near surface interference sources such as trees, power lines, railroad tracks, or any other type of utilities, as they might effect the radar (Figure 5). The test line should pass over ground that is typical in topography and subsurface conditions present in the projected profile area. Running the test line over a target of known depth will be useful in determining the velocity. Measuring electrical properties with an electrical parameters probe is also useful. Although these two means of data gathering are not always available or possible. Test lines should be considered as a calibration line that is to be re-run at periodic times during the day or when any changes in equipment are made.

Calibration of the recorder and the electronics should take place while running the test lines. Everything should be checked at this time to assure that the data received is correct and clean as possible. Running all of the available antennas along the test line will also help assure the "cleanest", least erroneous data is achievable.

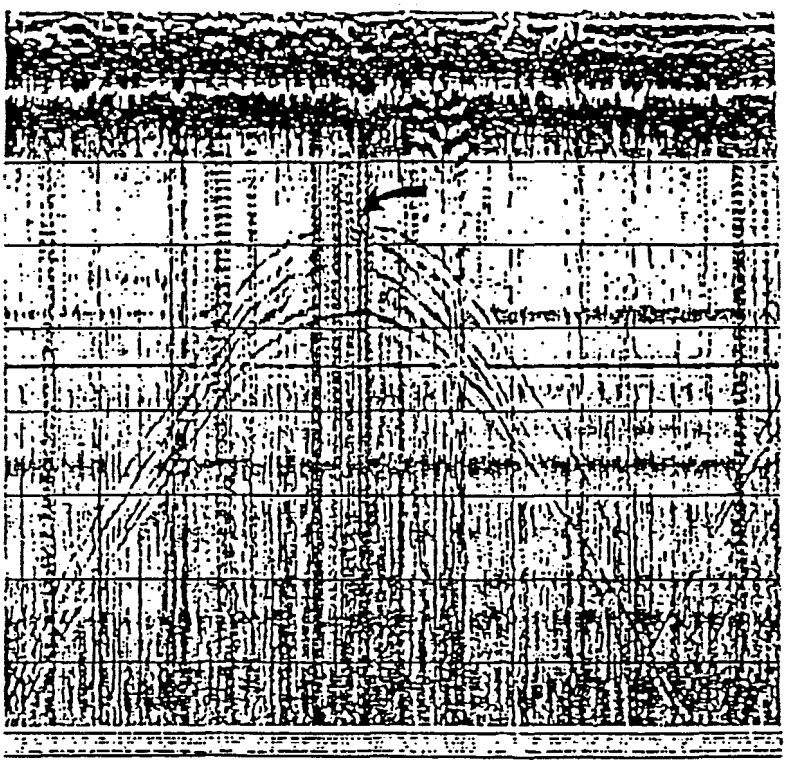

Figure 5. GPR record showing noise from passing under a powerline, with profile perpendicular to direction of powerline. Apex shown by arrow. Microwave antenna noise is also present on the record. (80 MHz, Northern Illinois).

(Daniels, 1989)

Selecting a means for towing the antenna is the simplest decision to make. It should be towed by something that is not going to interfere with the radar. In selecting what to use, the topography, the size of the area, and what is being surveyed will determine should be used to move the antenna. Usually an mobile or some type of ATV will suffice, or if the area is small enough, one can move the antenna by hand.

Deciding on a profile or grid pattern should be the next decision made. Of course, money and time are the primary deciding factors. The profile lines need to cover the survey site but not so much as to over-sample the site. Profile lines should be run perpendicular to the trend of the target. If the trend of the target is not known then a grid of profile lines must be established (See Figure 6., Daniels, 1989).

The survey is now ready to be run, as long as the area has not been determined as a "no-data-area" (i.e., no received reflections) (Daniels, 1989).

After the data has been gathered it is important to re-run the test lines to assure that the same results are achieved. This step is somewhat similar to "tie-ins" that are done during magnetic surveys, but for GPR, these are re-run to check for any changes that might occur to the equipment during the survey.

Sometime during the survey it is important to measure the electrical properties of the near-surface with a radio frequency probe, both on the test line and in the survey area. This will help in the calculation of the dielectric permittivity, wave velocity, and depth.

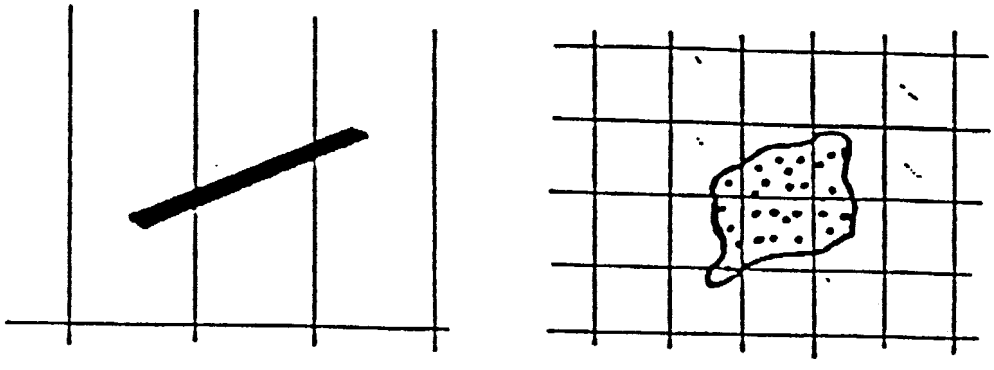

(a) Profile lines for 2-D targets. (b) Profile lines for 3-D targets.

Figure 6. Surface line setup for: (a) profiles across linear targets, and (b) a grid of profiles.

(Daniels, 1989)

Determination of the velocity from a buried target at a known depth can now be determined by using the following equation from Daniels and Roberts, (1994) Depth = two-way travel time/2x(velocity of the wave) or by using Velocity = Velocity of a radar wave through air/(relative permittivity of the material)$^{1/2}$

Data reduction is limited compared to reduction that is available to seismic data. GPR reductions are as follows from Daniels, (1989):

1) fairly simple filtering operations to remove unwanted noise on a scan-by-trace basis,

2) stacking (gathering and adding) adjacent scans to reduce random noise,

3) corrections for elevation changes, and

4) rubbersheeting.

After all of the above steps have been accomplished, the surveyor is now at what could be considered the most difficult point of the survey; identification of reflections. Identification of significant anomalies on GPR records is a pattern recognition process that consists of recognizing features on the records that are characteristic of known signatures (Daniels, 1989). Identifiable features on a radar record fall into three main categories:

1) Continuous reflections from horizontally layered geologic horizons.

2) Reflections from two- and three-dimensional objects.

3) Lateral discontinuities that cause an abrupt change in the signal amplitude, diffractions, or a termination of

adjacent reflections. (Daniels, 1989)

Continuous, layered, one-dimensional, boundaries are usually the most difficult features to identify on a GPR record, unless the boundaries are dipping. A reflection from a shallow horizontal boundary often interferes with other shallow reflections and ringing from the antenna (Daniels, 1989). Reflections from small two- and three-dimensional buried objects (buried pipes, lines, and barrels, etc.) can be identified by their small, characteristic, hyperbolic shapes (Figure 7., Daniels, 1989).

Lateral discontinuities can cause either a change in the trend of the continuous reflections, diffractions, or a change in amplitude and phase of the signal. A lateral change in amplitude and phase is often associated with changes in the surface impedance of the ground (Figure 8., Daniels, 1989).

Geological Applications

GPR is used in a variety of different situations, from identification of geologic to man-made/caused features. Applications fall into three main categories of identification:

1) host geology,
2) hydrogeologic features, and
3) man-placed features.

These include applications to groundwater, hazardous waste, and engineering (Daniels, 1989).

Applications to the host geology usually include investigations for dipping beds, stratigraphic changes, and the water table. We must remind ourselves that these features must

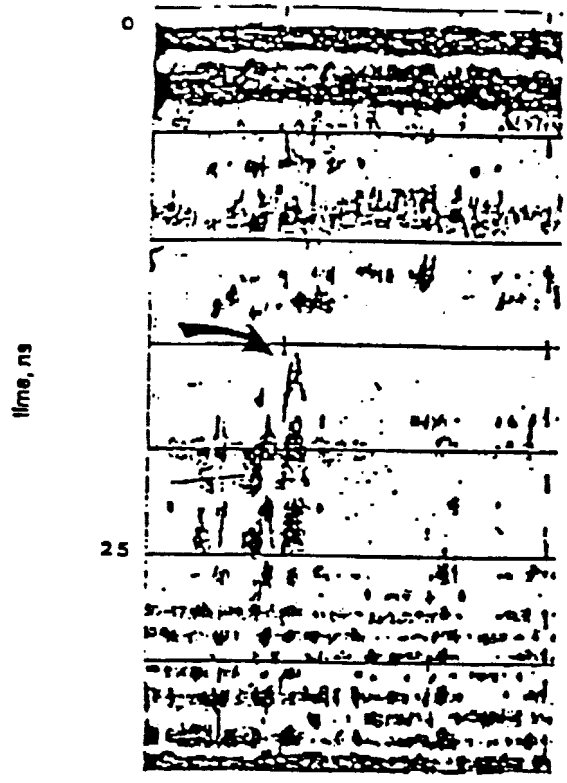

Figure 7. GPR record showing reflection from 1.2 cm diameter re-bar buried at a depth of 0.5 m (500 MHz, Southern Michigan, Clay soil).

(Daniels, 1989)

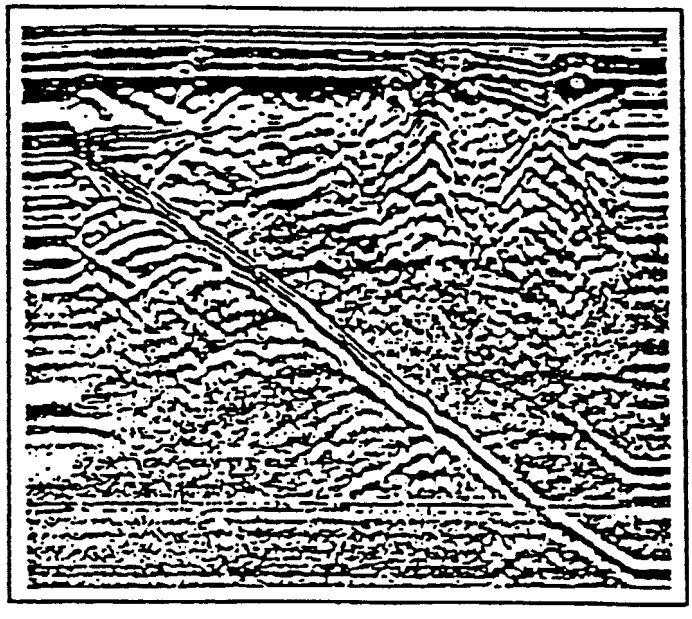

Figure 8. Diffractions caused by lateral discontinuity at depth [see arrows]

(Daniels, 1989)

produce a large enough contrast in conductivity and dielectric constant to yield a high reflection coefficient (i.e. change in rock type, porosity, or fluid saturation) (Daniels, 1989).

In terms of wave penetration, in general, clean sands, glacial material, and homogeneous acidic rocks will yield the best penetration and resolution (Daniels, 1989).

Lateral changes in electrical properties at or near the surface can cause changes in the transmitted signal and effect the entire GPR record (Daniels, 1989). A lateral change in surface materials (solids or liquids) is seen on the radar record primarily as a change in antenna coupling, which fundamentally effects the transmitted pulse and changes the response from reflectors below the surface (Daniels, 1989). This is important since GPR is used for the detection of hazardous wastes at or near the surface. Daniels, (1989), shows contaminant spills and their location can host a number of different problems (see Figure 9., (Daniels, 1989).

Two- and three-dimensional targets generally have hyperbolic diffraction patterns. These patterns are caused by the differences in travel times due to the shapes of the targets. The tops of the hyperbolas are caused by the immediate reflection of the electromagnetic waves. The legs of the hyperbolic diffractions are caused by the different reflection and arrival times of the electromagnetic waves off the sides of the targets. It is important to remember the types of diffraction patterns recorded from one type of target may not be the same in other survey areas. The differences may be in the electrical impedance of the ground,

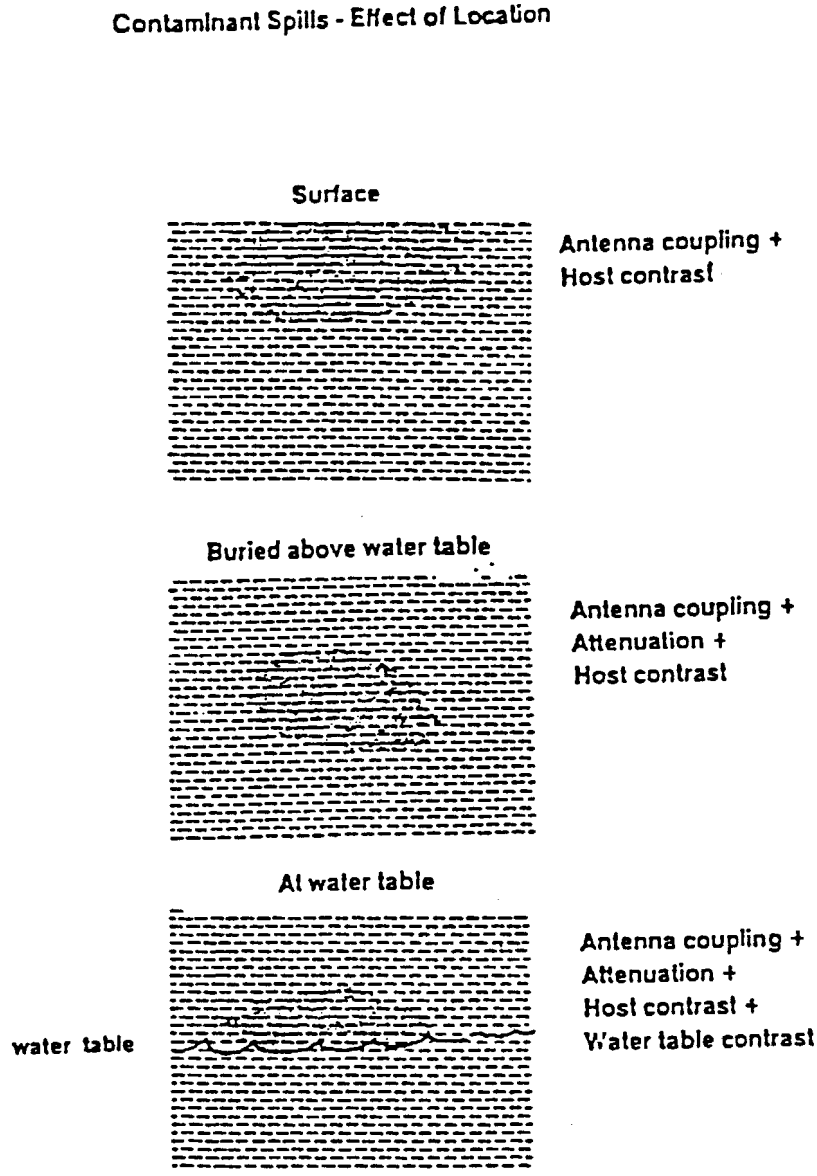

Figure 9. Three possible host locations for contaminant spills, and the resulting factors that must be considered when interpreting the GPR record.

(Daniels, 1989)

depth of target burial, and as Daniels, (1989) has shown, even variations of the water level in a pipe can effect the resulting diffraction patterns (Figure 10). The presence of an exact reflection from a certain type of target is unrealistic, but there is a basic type of target reflection to be found.

For the investigations in this thesis, the use of GPR was confined to the detection and identification of gasoline or hydrocarbon spills; including spills that occur at the surface, buried above the water table, and at the water table. Before moving into detection and interpretation of spills, we must first learn about the properties of these contaminants and how they behave on and in the ground.

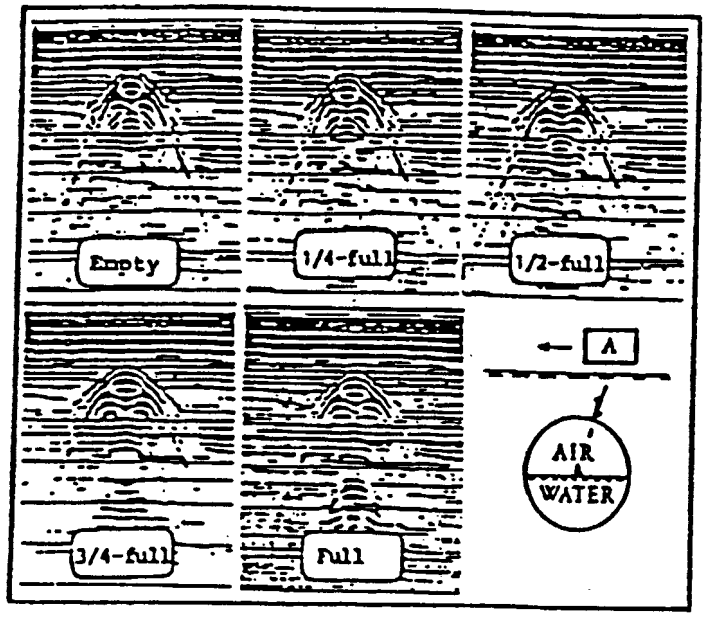

Figure 10. water "filled" pipe

Buried pipe containing various amounts of water

(Daniels, 1989)

Subsurface Contaminants

The Environmental Protection Agency (EPA) estimates that over 95 percent of the estimated 1.4 million Underground Storage Tanks (UST) systems are used to store petroleum products (Lyman and others, 1992). As a result of these numbers there are thousands of hazardous waste spill sites in the United States with organic compounds such as trichloroethylene, gasoline, and other solvents and fuels (Walther and others, 1986). Obviously these compounds, after coming into contact with the water table or with the environment pose a large hazard to our environment and especially to ground water supplies. Germany, for example, obtains more than four-fifths of its drinking water from the subsoil either as genuine ground water or as bank-filtered river water (Schwille, 1967). For each site, an understanding of the contaminant distribution and stratigraphy in three-dimensions is necessary for proposed cleanup processes (Walther and others, 1986).

> The EPA developed the concept that a substance leaking from an UST will be present in the transient between one or more locations or settings in the subsurface environment. A total of 13 locations, referred to as physicochemical-phase loci, were identified. Each of the 13 loci represents a point in space and the physical state of the leaked substance that together describe where and how these contaminants may exist in the subsurface environment after an UST release (Lyman and others, 1992).

After a UST leak has occurred and a contaminant has been dispersed it is important to remember that the contaminant will move between the different loci at varying rates depending on the surface and subsurface environment. Brief descriptions of these loci along with a schematic representation can be found in Table 1. and Figure 11. from Lyman and others (1992).

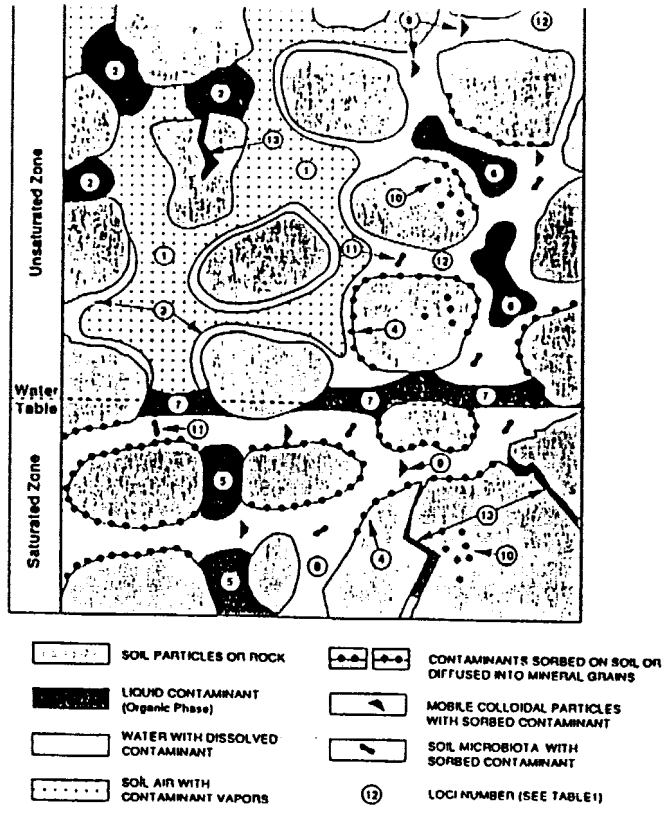

Figure 11. Schematic representation of the 13 loci in terms of unsaturated and saturated zones.

(Lyman and others, 1992)

Table 1. **Brief Descriptions of the 13 Physicochemical-Phase Loci**

Locus Number	Description
1	Contaminant vapors as a component of soil gas in the unsaturated zone.
2	Liquid contaminants adhering to "water-dry" soil particles in the unsaturated zone.
3	Contaminants dissolved in the water film surrounding soil particles in the unsaturated zone.
4	Contaminants sorbed to "water-wet" soil particles or rock surface (after migrating through the water) in either the unsaturated or saturated zone.
5	Liquid contaminants in the pore spaces between soil particles in the saturated zone.
6	Liquid contaminants in the pore spaces between soil particles in the unsaturated zone.
7	Liquid contaminants floating on the groundwater table.
8	Contaminants dissolved in groundwater (i.e., water in the saturated zone).
9	Contaminants sorbed onto colloidal particles in water in either the unsaturated or saturated zone.
10	Contaminants that have diffused into mineral grains or rocks in either the unsaturated or saturated zone.
11	Contaminants sorbed onto or into soil microbiota in either the unsaturated or saturated zone.
12	Contaminants dissolved in the mobile pore water of the unsaturated zone.
13	Liquid contaminants in rock fractures in either the unsaturated or saturated zone.

(Lyman and others, 1992)

Some terms important to these locations are as follows:

1) Diffusion - the movement of molecules (usually vapor) from an area of high concentration to an area of low concentration.

2) Advection - the movement of the soil gas caused by the effects of a pressure gradient exerted on the soil gas.

3) Colloidal particles - electrically charged particles (usually negative) that may be comprised of small solid particles, macromolecules, small droplets of liquids, or small gas bubbles.

4) Biodegradation - microbial organisms transform and alter the structure of contaminants that are introduced to the environment by enzymatic action.

5) Volatilization - The transfer of a contaminant from the liquid phase to the air phase.

A hydrological sub-division of the subsoil is illustrated in Figure 12. from Schwille, 1967.

All of the following loci information comes from Lyman and others, (1992).

Locus no. 1 contains contaminant vapors as a component of soil gas located anywhere in the unsaturated zone. The unsaturated zone is located anywhere above the water table, no matter what other structures may be present. The contaminants in this locus are quite mobile, moving via: a) diffusion through air pores (a concentration gradient-driven process), b) advection - which may be driven by density gradients, barometric pressure pumping, or sweep flow from in situ gas generation. Locus no. 1 originates from loci

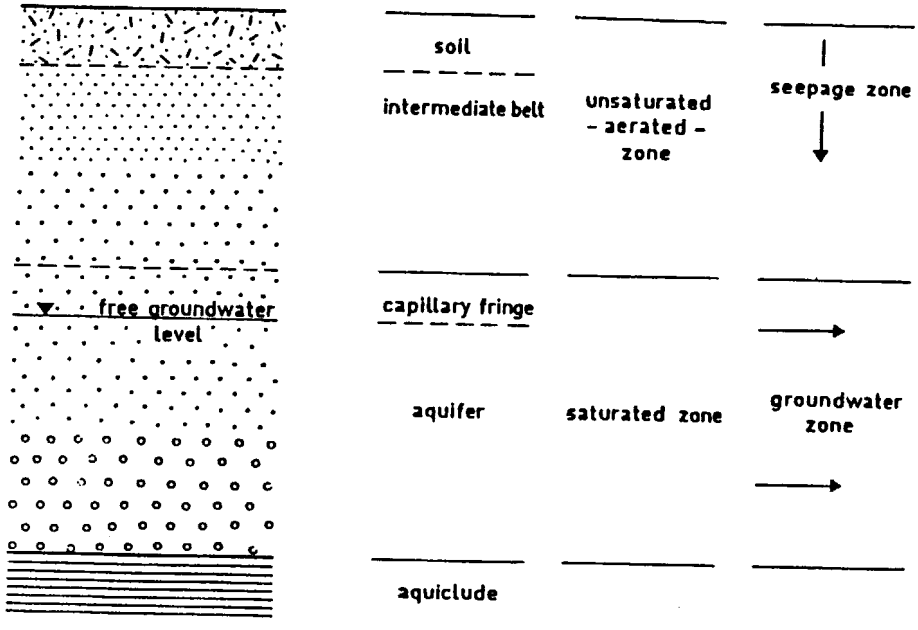

Figure 12. Hydrological sub-division of the subsoil (Schwille, 1967)

nos. 5, 6, and 7. The volatilized contaminant may then divide to locus no. 2 and 4. It may also dissolve into the water found in loci nos. 3, 12, and 8. Most loss of locus no. 1 comes from venting to the atmosphere.

Locus no. 2 contains liquid contaminants adhering to "water-dry" soil particles in the unsaturated zone. The contaminant in this location can be found as a continuous phase (e.g., in a spill front) or as a discontinuous phase (e.g., separate droplets), adhering to soil surfaces. Either phase is highly mobile from the effects of gravity, barometric pressure, water infiltration, and capillary tension. Locus no. 2 can greatly effect other loci depending on the amount of porosity present. Volatilization into locus 1, and dissolution into locus nos. 3 and 12 are the main loci effected by locus no. 2.

Locus no. 3 is made up of contaminants dissolved in the water film surrounding soil particles in the unsaturated zone. These are relatively immobile water films that can be found in a well-drained soil. This locus may intermix or advect with locus no. 12, volatilize into locus no. 1 and, sorption to locus no. 4 may also take place. This may seem like an unimportant loci but it may actually pose many problems. These problems include long retention times of the contaminant, contaminant loss due to bacterial action being reduced, and vacuum extraction is greatly impaired.

Locus no. 4 includes contaminants sorbed to "Water-Wet" soil particles or rock surface (after migrating through the water) in either the unsaturated or saturated zone. In this loci it is necessary for the contaminant to be first dissolved in water and

then secondly to be sorbed into the soil or rock surface. The contaminants are absorbed into a thin layer of naturally-occurring organic matter surrounding the soil particles, or absorbed in a thin layer to exposed mineral (e.g., clay) surfaces. These contaminants are therefore considered to be immobile, and are limited by the initial dissolution process. Locus no. 4 interacts with many of the other loci when hydrocarbons are sorbed onto soil surfaces, Table 2 lists the interactions of locus no. 4. The only process that is not considered significant is volatilization into the soil gas.

Locus no. 5 contains contaminants in the pore spaces between soil particles in the saturated zone. The contaminant in this loci is in the form of a liquid and it may either be the "Water-Wet" configuration (i.e., particle surfaces wet by water) or the "Oil-Wet" configuration (i.e., particle surfaces wet by oil); no air is present. The contaminants are likely to be present as a discontinuous phase, derived from a fluctuating water table level. Continuous phases are found to be a more likely contaminant such as tetrachloroethylene or PCBs. The liquid contaminant in locus no. 5 is considered to be relatively immobile and dissolution is the principle loss mechanism, due to density differences, buoyancy forces, and entrainment forces due to moving groundwater. Loci interactions of locus no. 5 can be found in Table 3., these list the processes, phases in direct contact, interacting loci, and the relative importance of each interaction.

Locus no. 6 contains liquid contaminants in the pore spaces between soil particles in the unsaturated zone. These contaminants

Table 2. Loci Interactions with Hydrocarbons Sorbed onto Soil Surfaces

Process	Phases In Contact	Interacting Loci	Relative Importance
Mobility			
Diffusion	Wet soil	3, 8, 9, 11, 12	Modest
Desorption	Wet Soil	3, 8, 9, 11, 12	High
Immobility			
Sorption	Rock	10, 13	Low

(Lyman and others, 1992)

Table 3. Loci Interactions with Residual Liquid Contaminant in Groundwater

Process	Phases In Direct Contact[a]	Interacting Loci	Relative Importance
Mobility			
Dissolution (Phase separation)	water	8	high
Bulk Transport (Displacement, Entrainment)	water	8	high
	wet soil	4	moderate
	rock	10	very low
	rock	13	high
	liquid hydrocarbon	7	high
Immobility			
Sorption	wet soil	4	moderate
	rock	13	low
Wetting Conditions	water	7, 8	moderate-high

a. Biota (locus no. 11) are potentially in direct contact with all phases.

(Lyman and others, 1992)

are in the "Water-Wet" configuration, (i.e, no substantial contact between liquid contaminant and the surfaces of the soil particles). Soil air is present and liquid contaminant-air interfaces exist. The mobility of liquid contaminants in this locus depends on the volume of the spill, its physicochemical properties, and the hydraulic properties of the porous medium (e.g., hydraulic conductivity, kinematic viscosity, and capillary tension). If a spill front from a large spill passes through the unsaturated zone, the contaminants may form a continuous phase. After the spill front has passed, a discontinuous phase is much more likely.

Interactions of locus no. 6 includes volatilization to locus no. 1 as the primary mechanism for partitioning. Loci nos. 3 and 12 may receive dissolved liquid contaminant from no. 6. This may then attenuate to soil particles of loci nos. 2 and 4. If the contaminant is in a large enough quantity or if it is mobile, it may move to loci nos. 7 and 8.

Locus no. 7 is made up of liquid contaminants floating upon the water table. Therefore the contaminant is less dense than water, although some high density liquids may also float upon the water table. If the amount of the contaminant is of sufficient quantity it may deflect the water table downward, this usually occurs directly below the leak. From this point the liquid contaminant will move laterally under the pressure of its own weight, or it will move down a sloping water table. A summary of loci interactions can be seen in Table 4. Locus no. 7 consists of the bulk of the liquid contaminant and is able to effect all of the other loci as it is highly mobile (shown in Table 4) especially

Table 4. **Loci Interactions with Liquid Contaminant Floating on Groundwater**

Interacting Locus	Phase Contacted	Transfer Process	Relative Importance
1	air	volatilization	high
2	dry solid	adhering	high
3	water	dissolution	moderate
5	water & solid	adhering	moderate
6	solid	adhering	high
8	water	dissolution	high
10	solid	adsorption	low
11	biota	sorption	moderate
12	water	dissolution	moderate
13	voids	bulk transfer	high

(Lyman and others, 1992)

nos. 1, 2, 6, 8, and 13. Losses are due to volatilization into air soil, dissolution into soil water, capillary retention, and dissolution.

Locus no. 8 includes contaminants dissolved in groundwater (i.e., water in the saturated zone), or groundwater contaminated with dissolved pollutants. Not to be confused with dissolution which is the process that takes place in loci nos. 2, 6, 7, and 5. In the saturated zone the contaminant is in a continuous phase and is highly mobile. The contaminant may flow in the vertical and horizontal directions. Flowing groundwater may carry the contaminant up to several kilometers from the site of the leak. A summary of loci interactions for locus no. 8 can be found in Table 5. Losses can be attributed to volatilization (loci no. 1), bulk transport (loci nos. 4, 10,and 13), and dissolution (loci nos. 2, 4, 5, 6, and 9).

Locus no. 9 contains contaminants sorbed onto colloidal particles in water in either the unsaturated or saturated zone. This locus is considered important in the fact that it allows for the mobilization of strongly-sorbed contaminants that would otherwise remain immobile due to sorption on a stationary phase. Loci interactions include 3, 5, 6, 7, 8, and 12 with attachment of contaminants onto colloidal particles in groundwater. Bulk transport into the locus occurs from locus nos. 3, 5, 6, 7, 8, and 12.

Locus no. 10 is defined as contaminants that have diffused <u>into</u> mineral grains or rocks in either the unsaturated or saturated zone. Capillary tension drives the contaminant into

Table 5.

Loci Interactions with Hydrocarbon Dissolved in Groundwater

Process	Phases in Contact[a]	Interacting Loci	Relative Importance
Mobility			
Dissolution	wet soil	4	low
	liquid hydrocarbon	5,7	high
Bulk Transport (advection and dispersion/ diffusion)	liquid hydrocarbon	5,7	high
	wet soil	4	moderate
	rock	13	moderate-high
	air	1	low
Volatilization			
Immobility			
Sorption	wet soil	4	low
	rock	10,13	low

a. Biota (locus no. 11) are potentially in contact with all phases.

(Lyman and others, 1992)

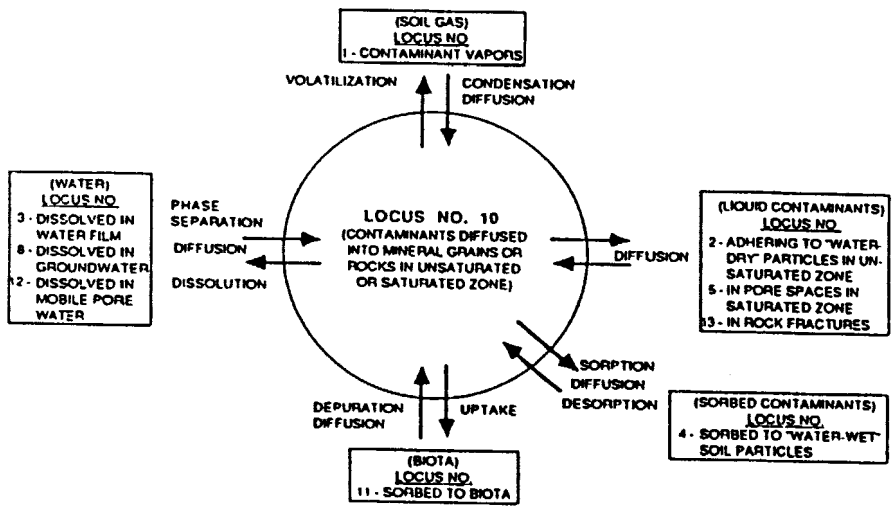

Figure 13. Schematic representation of important transformation and transport processes affecting other loci.

(Lyman and others, 1992)

microfractures, micropores or into thin spaces between mineral layers (e.g., clay platelet). Diffusion causes the contaminant to penetrate mineral crystals or amorphous solids. Loci interactions are extensive and can be found in Figure 13.

Locus no. 11 involves contaminants sorbed onto or into soil microbiota in either the saturated or unsaturated zone. Organic chemicals can be sorbed by soil microbiota by several mechanisms:

1) sorption to the exterior cell membranes or to excluded extracellular material;

2) molecular transport across the cell membranes into the cells' cytoplasm; or

3) ingestion of particles or liquid droplets.

Soil biota include bacteria, fungi, and yeasts, but only aerobic degradation is considered important for hydrocarbons. The concentration of biota in soil drops off significantly with increasing depth. The unsaturated zone is probably much more important than the saturated zone for biodegradation of hydrocarbons, but this is ultimately controlled by the environment in which the UST leak takes place. The controlling factor in biodegradation is found in the presence and availability of oxygen in the subsurface.

Locus no. 12 contains contaminants dissolved in the mobile pore water of the unsaturated zone. This includes water occupying a large fraction of the total porosity of the soil at certain times or places (e.g., after a heavy rainfall or above the capillary fringe). Dissolved contaminants, in the pore water, are moved by capillary tension and gravity. The primary mechanism for

partitioning into locus no. 12 is from dissolution of a liquid contaminant in locus no. 6. Contaminants may also:

a) partition into the air phase of locus no. 1;

b) soil particles may attenuate contamination by retardation and sorption (loci nos. 2 and 4);

c) migrate vertically, contaminating the groundwater (locus no. 8) and;

d) aided by mobile colloids (locus no. 9).

Locus no. 13 includes liquid contaminants in fractured rock or karstic limestone in either the unsaturated or saturated zone. Rocks with fracture zones or dissolution zones are typically very permeable, leaked product can travel very quickly from the spill site. Figure 14. shows a schematic representation of the major interactions among locus no. 13. The liquid contaminant is highly mobile and will interact with almost all other loci. The contaminant in this locus interacts in a variety of ways:

a) diffusion into loci nos. 2, 5, or 6;

b) gather as a free product lens (locus no. 7);

c) contaminant may absorb onto the rock face (locus no. 4);

d) contaminant may be absorbed to micells travelling through the fractures (locus no. 9);

e) biodegradation and inorganic transformations may occur in this locus;

f) volatilization (locus no.1);

g) contaminants dissolved in water (locus nos. 3, 8, or 12). The interactions with loci no. 13 as stated before are shown in Figure 14.

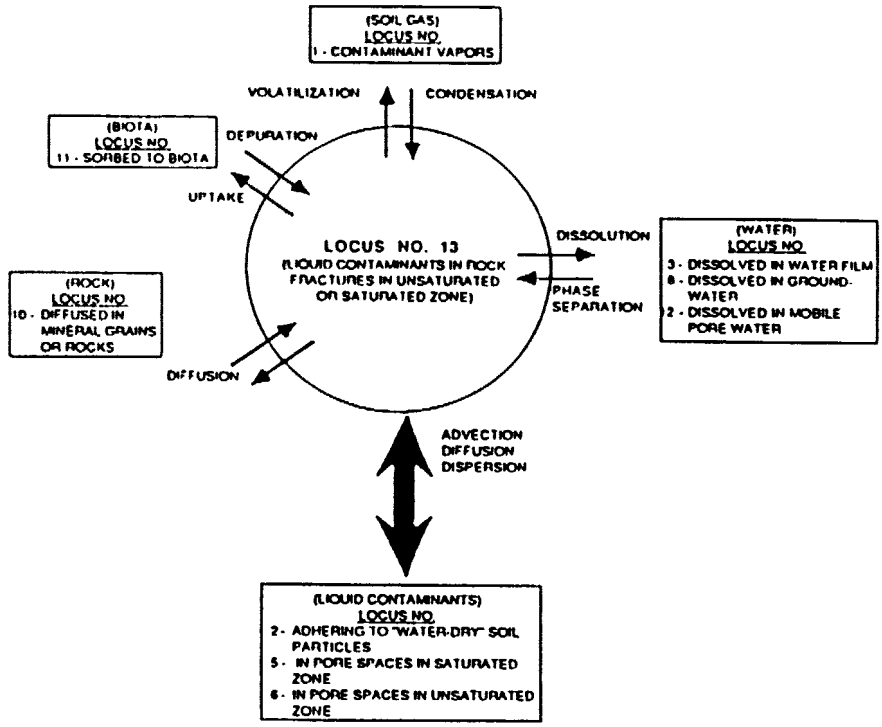

Figure 14. Schematic representation of important transformation and transport processes affecting other loci.

(Lyman and others, 1992)

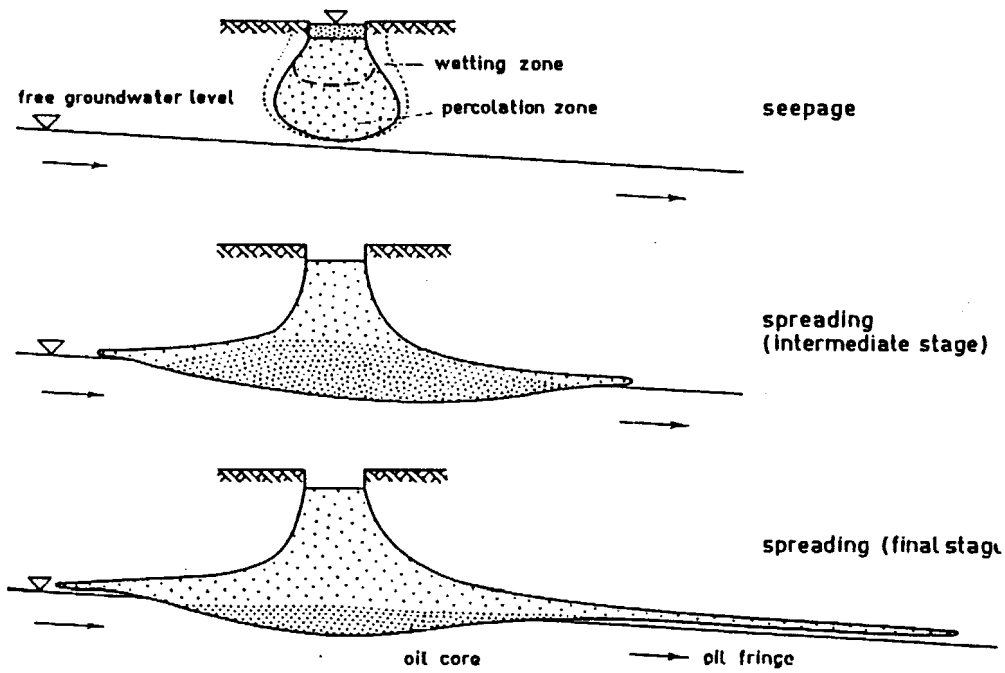

Figure 15. The spreading of oil in a porous medium (schematically)

(Schwille, 1967)

Looking at the migration of a spill in a larger picture, Schwille, (1967), groups the migration of "oil" (referring to crude and its liquid derivatives) into three phases:

a) Seepage - principally downward vertical movement of oil in the unsaturated pore spaces;

b) Lateral spread - migration along the border between the unsaturated and the saturated pore space or on stratum surfaces, mainly horizontal: and

c) Drift - the passive movement, on the groundwater surface, of the body of oil which is still spreading, or has already attained its maximum lateral extent.

(The three phases are shown in Figure 15. of Schwille, 1967). Transitional locations between these three phases are listed within the 13 loci above.

Detection of Contaminants in the Field.

The detection of organic contaminants has been proven with only three geophysical techniques - conductivity, complex resistivity, and ground penetrating radar; although none of the techniques works successfully in all environments (Olhoeft, 1986).

Ground penetrating radar (GPR), has been shown in a variety of laboratory experiments and real-life uses to be a valuable technique for detection of many subsurface contaminants. GPR works like most electrical geophysical methods. The system is able to pick up the different electrical properties present in pore spaces that are filled with air, groundwater, and contaminants. The presence of hydrocarbons and organic chemicals bring about

significant changes in the electrical properties of soils in the GPR frequency band of 10Mhz to 1Ghz, and detection of free product gasoline using GPR is possible (Redman, and others (1991). GPR will readily measure the presence of water-insoluble contaminants that float on the water table, and it is able to map some hydrocarbon contaminants (Olhoeft, 1986).

Most literature on the topic of subsurface contaminants groups them into two groups:

1) DNAPLs - Dense Non-Aqueous Phase Liquids.

2) LNAPLs - Light Non-Aqueous Phase Liquids.

DNAPLs, are highly unpredictable due to their density, low viscosity, and low solubility, and will penetrate through the water table and may flow along with the groundwater. At the same time dissolving into a highly toxic state. For geophysics, DNAPLs can also be considered as nonconducting, nonpolar materials that increase formation density, and decrease conductivity and permittivity (Annan and others, 1991). Immediately one should realize that there will be obvious differences in the dielectric records of the two zones, which should in turn show up on the GPR records, although it is stated by Annan and others, (1991) that DNAPLs are difficult to detect in the subsurface.

In zones where DNAPL pooling has occurred large changes (on the order of 20%) have been observed in the dielectric permittivity, and it also produced detectable radar reflections (Redman and others, 1991). This radar reflection can be attributed to the fact that the presence of a DNAPL will reduce the dielectric permittivity of the soil and increase the wave propagation

velocity. On the other hand, it is important to remember that an increase in the dielectric permittivity will cause a decrease in propagation velocity. Redman and others, (1991), also stated that reflection travel time decreased by about 5ns during the time that they surveyed a spill site.

LNAPLs contaminants are reasonably predictable, less dense than water, and usually pool on top of the water table. These highly volatile contaminants (gasolines) evaporate rapidly. Being heavier than air, they form a jacket of hydrocarbon vapors (or evaporation envelope) that can be found in the large pores directly above the capillary fringe (Figure 16. Schwille, 1967). It should be noted that LNAPLs may sometime penetrate the water table due to the subsurface environment or the amount of the liquid spilled, and they will flow on top of the water table (Figure 17., from Dietz, 1967). Bruell and Hoag, (1986) state that vapor diffusion is significant in the movement of gasoline-range hydrocarbons within groundwater systems, especially within the vadose (unsaturated) zone.

Figure 18. from Daniels, (1989) shows two GPR lines and a product-thickness map from a survey area where gasoline has leaked from storage tanks on the surface.

> Arrows on the product-thickness map show the theoretical direction of product flow towards collector wells. The interpretated water table is located at a depth of approximately 60ns. Zones on the radar records containing numerous small scattering anomalies are interpreted as the locations for maximum product. This interpretation is based on the hypothesis that the gasoline product is accumulating in small localized "pods", which act to scatter the radar signal. Hence, most of line 6 is free of large quantities of product at the surface of the water table, while most of line 3 contains product above, or near, the water table. It should also be noted that contaminated

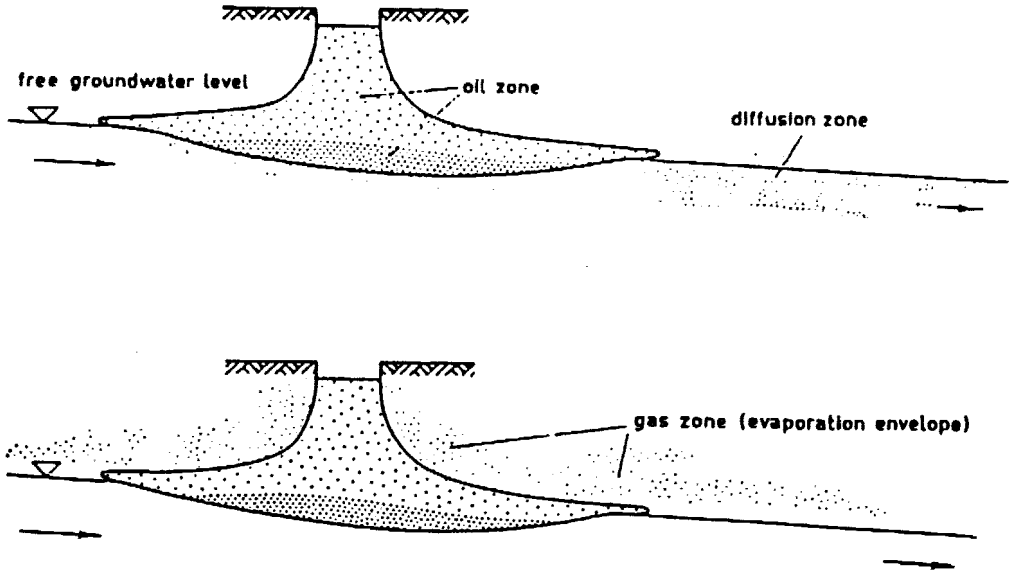

Figure 16. The distribution of oil, dissolved and gaseous hydrocarbons in a porous medium (schematically)

(Schwille, 1967)

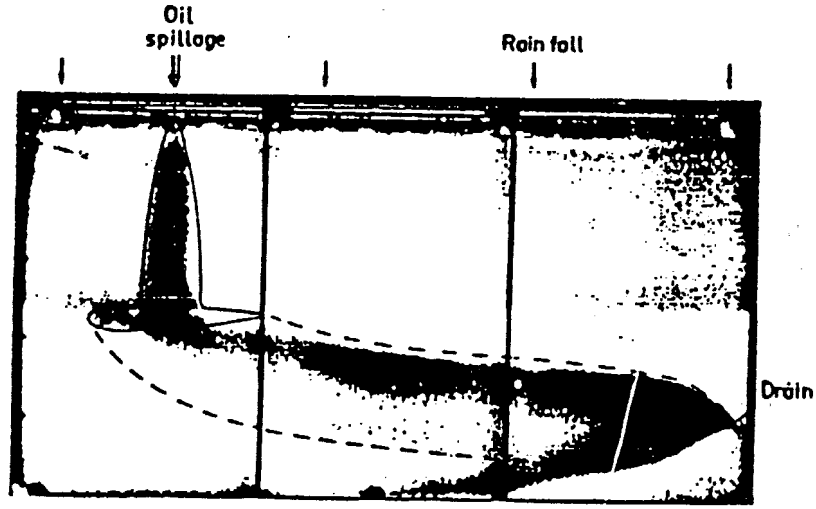

Figure 17. Model experiment of ground-water flow, showing the water stream that carries oil components.

(Dietz, 1967)

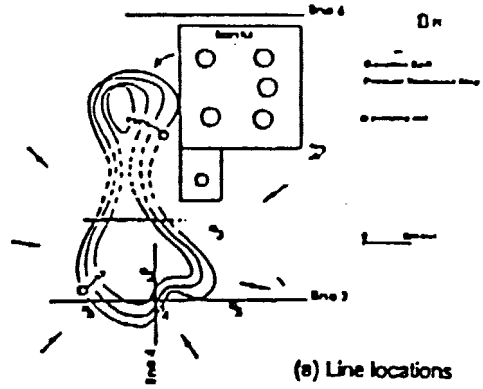

(a) Line locations

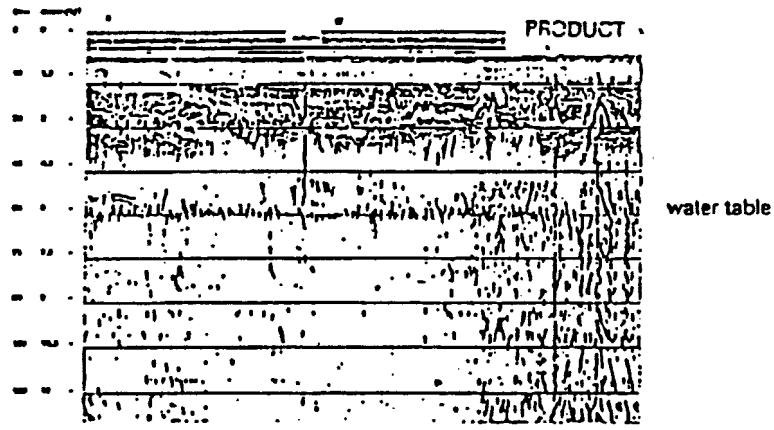

(b) Line 6

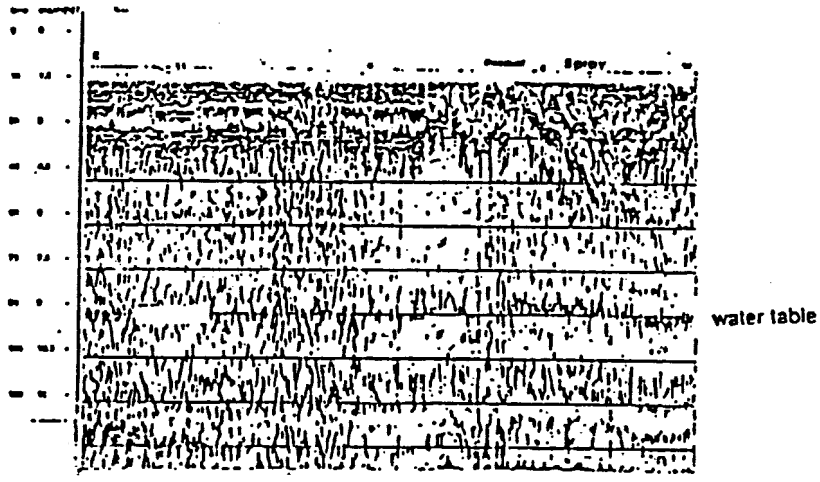

(c) Line 3

Figure 18. Results of GPR survey across an area where gasoline was leaked from surface tanks. (a) product-thickness map of the area, (b) GPR line 3, and (c) GPR line 6. (80 MHz, monostatic)

(Daniels, 1989)

water is continously being sprayed into the air in the region marked "spray" on line 3 (Daniels, 1989).

Figure 19. from Olhoeft, (1989) is a portion of a GPR record from a spill site in Minnesota. An observer of the record should be able to immediately notice that the right and left sides of the record are definitely different. The left side of the record is illustrative of the normal reflection of the site. The right side of the record is almost featureless, due to the oil that is floating on the water table. The oil and the material that it is saturating (mostly glacial outwash) have nearly the same dielectric permittivity and electrical conductivity. Therefore, little or no contrast exists to allow the radar to measure changes (Olhoeft, (1989). At first this sounds bad, in terms of using radar for hydrocarbon detection, but by looking at the left side of the record one sees that there are large contrasts. These contrasts are caused by differences in porosity, and in the amount of water content in the outwash. Thus, these changes are detectable to the radar. In other words, GPR measures differences of dielectric permittivity and conductivity. Approximate conductivity and dielectric values of some materials are shown in Table 6. from Beres and Haeni, (1991). As a reminder, low conductivity materials result in wave penetration of up to 30m (i.e., glacial outwash), and high conductivity materials result in low wave penetration <3ft (i.e., soil high in clay content). High clay content also causes high permittivity thus, low wave propagation velocity and penetration. Low clay content results in low permittivity, thus high wave propagation velocity and penetration. The example from Olhoeft, (1986) should also make it apparent that not only is GPR

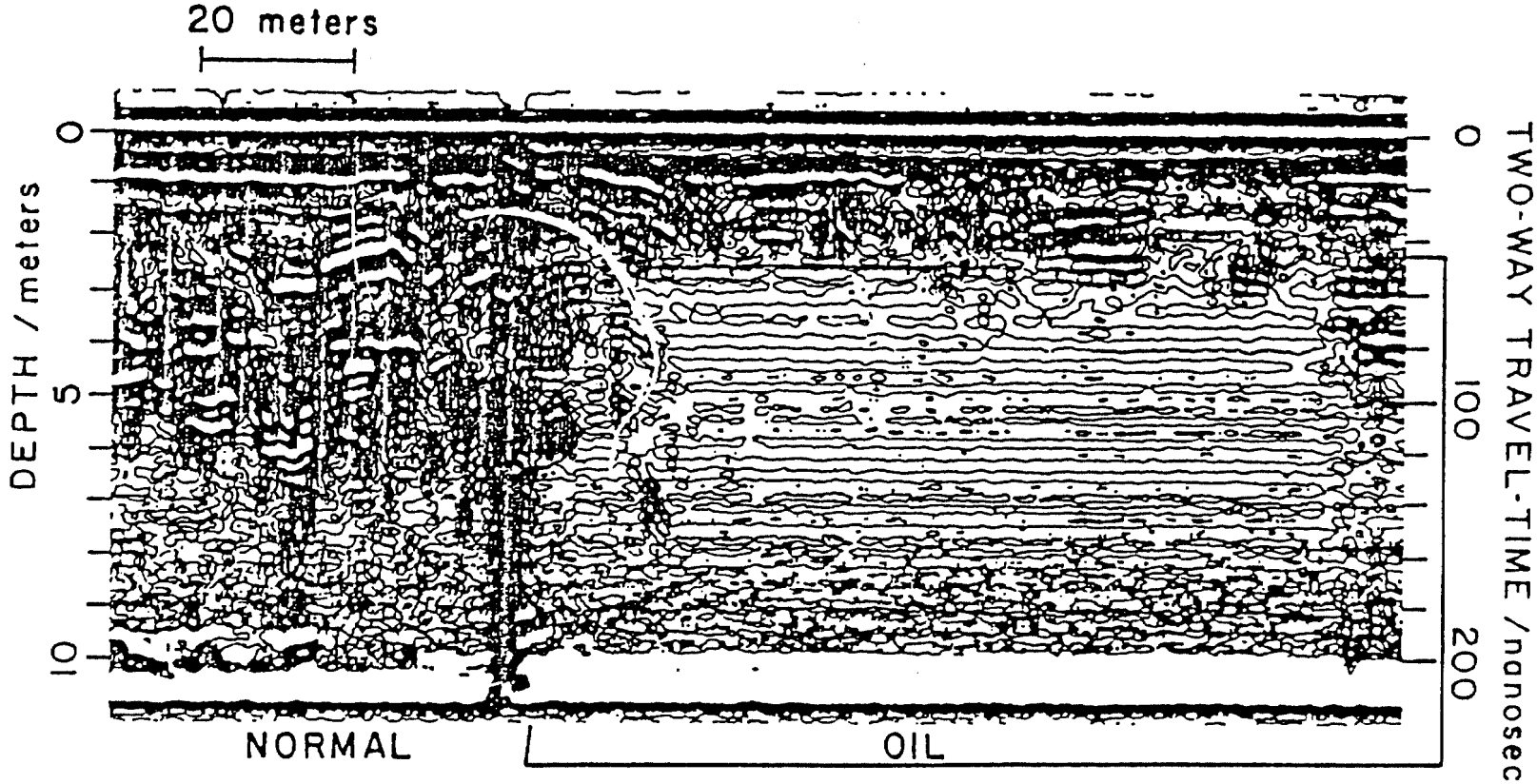

Figure 19. - Ground penetrating radar record (80-MHz center frequency, impulse monostatic) over the petroleum pipeline spill near Bemidji, Minnesota. Note the dramatic change in the texture of the record in the right half where oil is floating on the water table. The depth scale on the left is aproximate. Note the vertical exageration.

(Olhoeft, 1986)

Table 6. **Approximate Values of Conductivity and Relative Dielectric Permittivity for Selected Materials**

Material	*Conductivity (mhos per meter)*	*Relative dielectric permittivity*
Air	0	1
Pure water	10^{-4} to 3×10^{-2}	81
Sea water	4	81
Fresh-water ice	10^{-3}	4
Sand (dry)	10^{-7} to 10^{-3}	4 to 6
Sand (saturated)	10^{-4} to 10^{-2}	30
Silt (saturated)	10^{-3} to 10^{-2}	10
Clay (saturated)	10^{-1} to 1	8 to 12
Sandstone (wet)	4×10^{-2}	6
Shale (wet)	10^{-1}	7
Limestone (dry)	10^{-9}	7
Limestone (wet)	2.5×10^{-2}	8
Basalt (wet)	10^{-2}	8
Granite (dry)	10^{-8}	5
Granite (wet)	10^{-3}	7

(Beres, Haeni, 1991)

a useful tool in detection of contaminants, but it is also excellent for illustrating the hydrogeology and structure of the subsurface.

The following experiment was conducted at the Ohio State University, behind the Electroscience Laboratory during the month of March, 1994. The experiment is a portion of a larger experiment being conducted by David Grumman, a Masters student at The Ohio State University.

Purpose of Experiment

The purpose of the following experiment is to test the results of a Ground Penetrating Radar (GPR) system in a controlled hydrocarbon environment. This experiment was conducted in order to answer questions regarding exactly which contaminant zone the GPR system actually detects (i.e., gasoline saturation, vapor, etc...). The experiment was designed so an acrylic tank of sand could be changed from containing dry sand, to containing sand and free-product gasoline, to containing sand, gasoline, and water. Each environment was surveyed to determine if the GPR would detect the gas saturated zone, gas capillary fringe, or gasoline vapor above the unsaturated zone. Water was then added to observe the resulting effects on the GPR records. Changes in wave velocity, dielectric permittivity, and conductivity were expected to be observed on the GPR record. Therefore, due to the above changes, resolution, wave penetration, and reflections should also show some type of effect.

Experimental Methods

A clear acrylic tank with the dimensions of 4ft.x 3ft.x 4ft. was constructed in order to hold a homogenous sand mixture (Figure

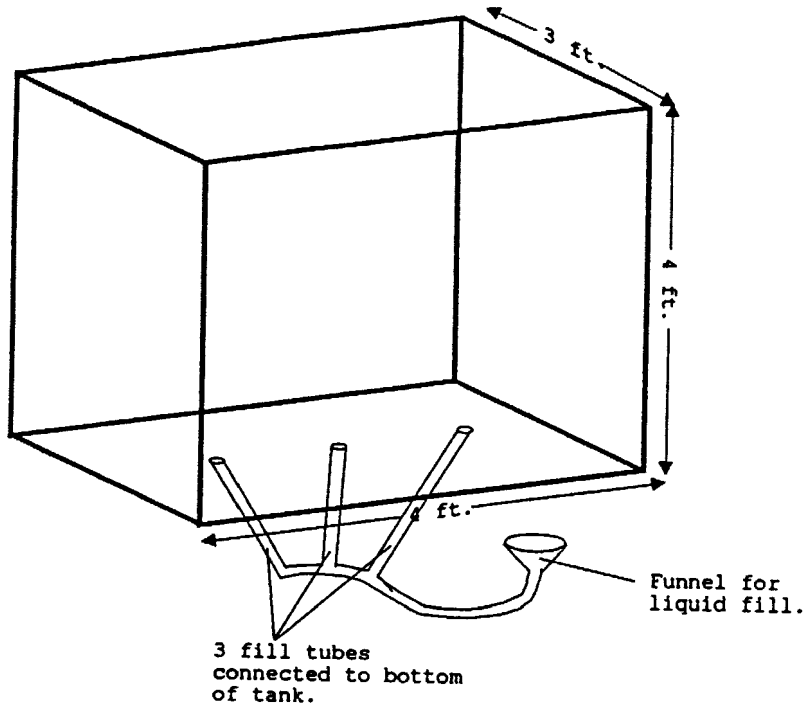

Figure 20. Illustration of sand tank that was constructed for the experiment

20). The acrylic was purposely chosen as the tank material to enable one to see exactly where the zones of saturation, vapor, etc., occurred. The tank was also equipped with three separate valves located on the bottom panel. These valves were connected to three hoses which enabled the experimenters to fill the tank (with gas and water) from the bottom up. Small screens were placed over the valve openings to keep the sand mixture from entering. The bottom of the tank was also kept from coming into contact with the ground by being placed into a wooden cradle.

The tank was first filled evenly with 1-1.5 inches of pebble-sized gravel. The rest of the tank was then filled with a dry, coarse to very coarse grained sand. The sand was packed down with a flat sledge, roughly every 8-9" (inches). The top 1 and 1/2 feet was not packed with the sledge. The top was then smoothed-out and another thin sheet of acrylic was placed on top to keep any unwanted moisture from entering the system. The framing on the top of the tank was slotted to ensure the antennas would pass over the same profile lines during each phase of the experiment. The framing on the side of the tank was fitted with shelving brackets, also in order to ensure the same lines were being surveyed. A line (i.e., fishing line) was used to connect the antenna and pull it across the tank and at the same time, trigger the recording system. The tank was then left to equalize overnight.

Two antennas (a 500Mhz and a 900Mhz) were used for the experiment. First, test and calibration lines were run in order to assure the equipment was working properly and the data was "clean" as expected. Calibrations were executed by holding the antennas to

the side of the tank and approaching the opposite side with a metal target. These calibrations proved useful in determining the velocity of the material for the radar wave, permittivity of the material, and in locating exactly where the back of the tank was located on the GPR records. Calibration lines were also run by moving the antennas and targets from the top to bottom of the tank vertically. These were run to observe any changes that occur from the top of the tank to the bottom of the tank. After both antennas were calibrated and test lines were run, the 500Mhz antenna was re-calibrated and the survey began. First, depending on which antenna was used, roughly 22-29 lines on the top of the dry sand tank were run. Secondly, approximately 16-18 lines on the side of the tank were run. Next, the 900Mhz antenna was calibrated and the survey followed the same procedures as for the 500Mhz antenna.

Fifteen gallons of gas were added to the tank system from the valves and tubes located in its bottom. Even though the gas filled from the bottom up, the tank was allowed to equalize overnight. After equalization, gasoline saturated roughly 1-1.5" of the tank, with a 0.5" capillary fringe above the saturation zone. Both antennas were calibrated again utilizing the exact method as before, and the survey lines were conducted. During the testing, it was observed that a strong gasoline vapor was escaping from under the top sheet of acrylic, indicating the gasoline was undergoing movement by diffusion and advection (see description of locus no. 1).

Fifteen gallons of water was then added to the system through the valves and tubes located in the bottom of the tank. The tank

system was then allowed to equalize overnight. Dye was placed into the added water, but it was only noticeable in the gravel located in the bottom of the tank. Addition of the dye was done in an attempt to show separation of the water saturated zone and the gasoline saturated zone. After equalization, it was estimated that water saturated 1.5-2.5" of the bottom of the tank. Since gasoline is less dense than water, the 1-1.5" of gasoline was floating on top of the water table. A small capillary fringe (approximately 0.5") was also observed. Antennas were once again calibrated and the survey lines were executed.

Another thirty gallons of water was added, but this time from the surface of the tank in an attempt to produce a slug. The test resulted in a large amount of water percolating down through the sand, gas, and water. This inevitably resulted in displacement of the gas floating on the water and possibly some "mixing" of the gas and water. Calibrations were conducted as before, then survey lines were run, also (as before) with both antennas. The tank was allowed to equalize overnight and another set of lines were run the following day.

The water saturation was located in the bottom 6-7", followed by a 4" capillary fringe (most likely containing water and gas). After survey lines were run on this last test, a dielectric probe was used in order to compare the measured and calculated dielectric permittivity values. The measured dielectric values are located in Tables 7 and 8.

At the end of the experiment, the equipment was packed and the contents of the tank were emptied into a hazardous waste container.

Estimated Conductivity and Dielectric Permittivity at 40 MHz only, Probe Holes #1 & #2

Probe Hole #1	40MHz Conductance (m-mhos/m)	Relative Permittivity
Depth	$\mathrm{Re}(\sigma 40_k)\cdot 10^3$	$\mathrm{Re}(\varepsilon 40_k)$
5"	14.877	11.088
8"	14.489	10.943
11"	18.314	13.138
18"	19.227	13.942
21"	18.772	13.735
24"	19.223	13.529
29"	13.794	10.97
35"	22.673	15.068
41"	22.65	15.549
45"	28.23	19.076

Table 7.

Probe Hole #2 (ignore '60 MHz' references)	40MHz Conductance (m-mhos/m)	Relative Permittivity
Depth	$\mathrm{Re}(\sigma 60_{kk})\cdot 10^3$	$\mathrm{Re}(\varepsilon 60_{kk})$
6"	7.837	7.272
12"	7.388	7.322
18"	7.216	7.445
24"	6.472	6.908
30"	8.155	7.899
36"	23.202	14.828
42"	33.38	19.618
46"	27.748	18.123

Table 8.

The stored raw data was then transferred to The Ohio State University geophysics lab for processing. The data was processed on programs developed by Dr. Jeffery J. Daniels and his graduate students at The Ohio State University.

Interpretation and Conclusions

The calibrations were the first data set to be processed. These calibrations proved to yield the most useful information about the characteristics of a GPR signal through certain medias. Calibrations for the 500Mhz and 900Mhz antennas are located in the following Figures. Parameters for the calibrations are located in the Tables immediately following these Figures. The equations used for calculation of two-way travel time, wave velocity, and dielectric permittivity are as follows. Two-way travel time (t_2); t_2 = [Total range of scan / Total sample (inches)] x change in samples (inches), t_2 units in nanoseconds (ns). Velocity (V); V = [2 x Distance (meters) / t_2] x [1/1x10^{-9}], V units in meters per second (m/s). Dielectric permittivity (E_r); E_r = [Speed of light in free space / V]^2.

Figure 21 shows the GPR signal received, in dry sand, for the 500Mhz antenna and Figure 22 for the 900Mhz. Both records show there are strong reflections present from the metal target at the back side of the tank. Tables 9-10 illustrate the parameters of the calibrations, including two-way travel time in nanoseconds (ns), velocity at 10^8 m/s, and the calculated dielectric permittivity. On comparison, it should be noted that both antennas yield excellent results. The two-way times, velocities, and

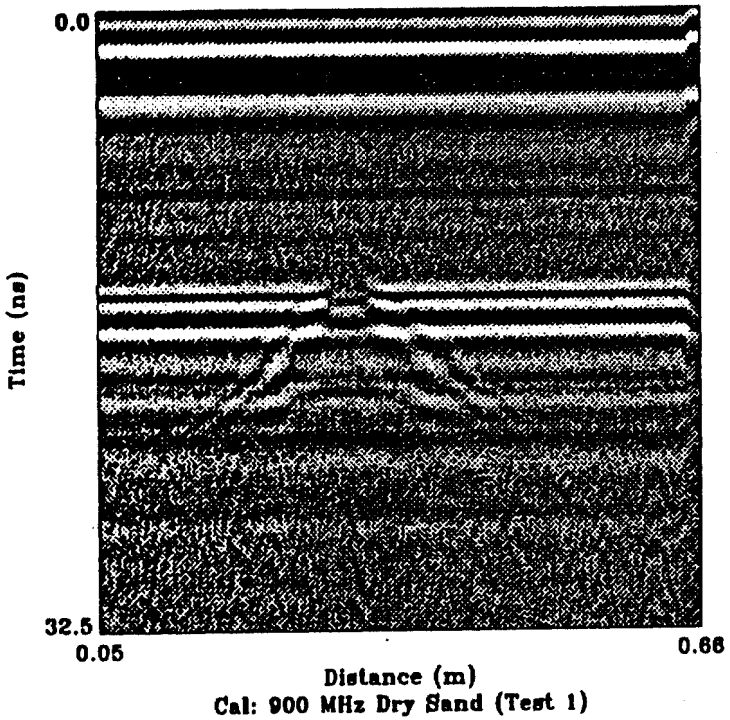

a) calibration of 900Mhz antenna for dry sand

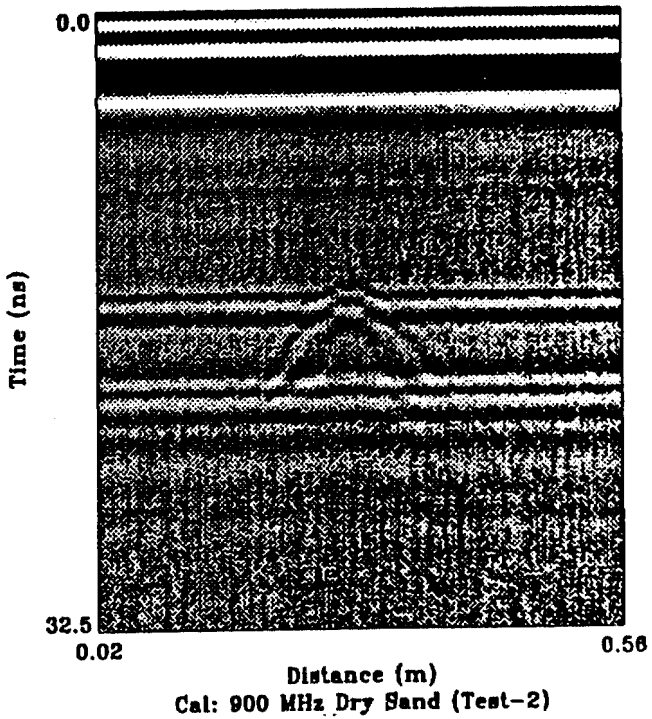

b) calibration of 900Mhz antenna for dry sand

Figure 22.

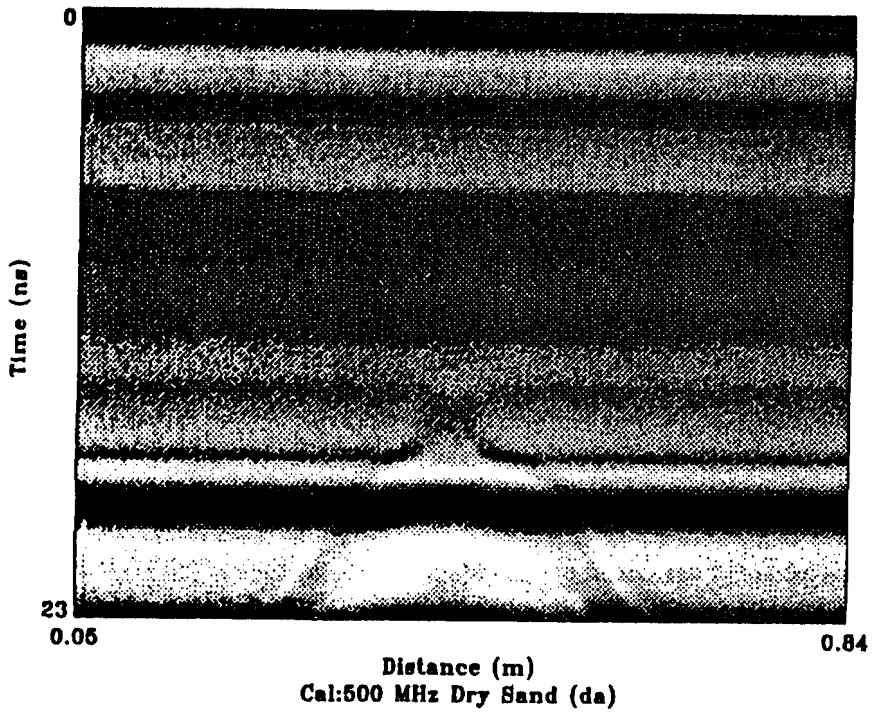

a) calibration of 500Mhz antenna for dry sand

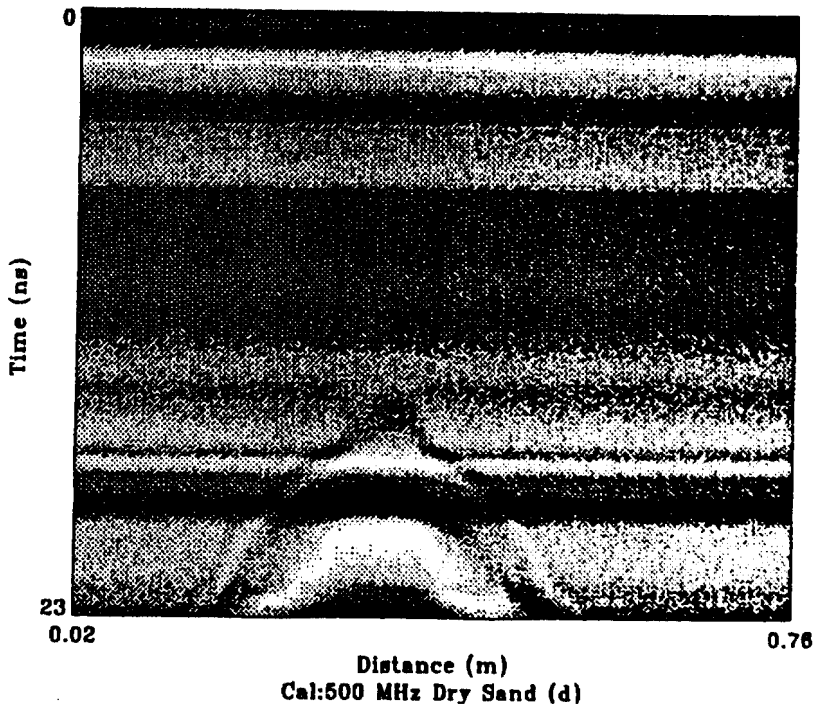

b) calibration of 500Mhz antenna for dry sand

Figure 21.

File Name	cal500d.parm	File Name	cal500d.parm
DC Offset	32767	DC Offset	32767
Range (ns)	23	Range (ns)	23
Upper Amplitude Cutoff	196	Upper Amplitude Cutoff	60
Lower Amplitude Cutoff	60	Lower Amplitude Cutoff	196
Top Sample Displayed	118	Top Sample Displayed	118
Bottom Sample Displayed	1023	Bottom Sample Displayed	1023
Number Of Samples/Trace	1024	Number Of Samples/Trace	1024
Two-Way Time (ns)	14.327	Two-Way Time (ns)	14.327
Velocity (m/s)	1.276*10 8	Velocity (m/s)	1.276*10 8
Dielectric Permittivity	5.52	Dielectric Permittivity	5.52

Table 9. Parameters for
500Mhz antenna for dry sand

File Name	cal900d.parm	File Name	cal900d.parm
DC Offset	32767	DC Offset	32767
Range (ns)	32.5	Range (ns)	32.5
Upper Amplitude Cutoff	176	Upper Amplitude Cutoff	176
Lower Amplitude Cutoff	80	Lower Amplitude Cutoff	80
Top Sample Displayed	99	Top Sample Displayed	99
Bottom Sample Displayed	1023	Bottom Sample Displayed	1023
Number Of Samples/Trace	1024	Number Of Samples/Trace	1024
Two-Way Time (ns)	14.258	Two-Way Time (ns)	14.258
Velocity (m/s)	1.282*10 8	Velocity (m/s)	1.282*10 8
Dielectric Permittivity	5.45	Dielectric Permittivity	5.45

Table 10. Parameters for
900Mhz antenna for dry sand

dielectric permittivities are essentially the same for both antennas (note differences in range for Figures 21 and 22).

With the addition of 15 gallons of gasoline, noticeable differences show up on the GPR records. As the antennas are moved down the side of the tank, contrasts in wave velocity and dielectric permittivity become more apparent. Figures 23-25 and Tables 11 and 12 illustrate the differences in wave velocity and dielectric permittivity. The records from the top of the tank are essentially the same as found in the 500Mhz and 900Mhz dry sand calculations. The bottom of the tank (i.e., gas saturation) now yields wave velocities in the order of 5.00×10^6 m/s faster than what is found in the dry sand. No doubt this result is directly related to the dielectric permittivity (E_r) of the two medium. In short, for the 900Mhz antenna, gasoline saturated sand (i.e., bottom) $E_r = 5.06$, dry sand (i.e., top) $E_r = 5.44$ (Table 11); for the 500Mhz antenna, gasoline saturated sand $E_r = 5.06$, dry sand $E_r = 4.40$ (Table 12). It should be noted that, the dielectric permittivities are somewhat different for the two antennas. Figure 25 illustrates how the velocities, thus travel times (i.e., reflections) are affected as the antenna moves from the bottom of the tank to the top (i.e. left to right). The record appears to be caused by dipping stratigraphic beds, but is actually caused by increased wave velocities in the bottom of the tank.

The introduction of water to the system also greatly influenced the velocities and dielectric permittivities, thus arrival times of the waves. Velocities were reduced on the order of 5.73×10^7 m/s as the antenna was moved from the bottom of the tank

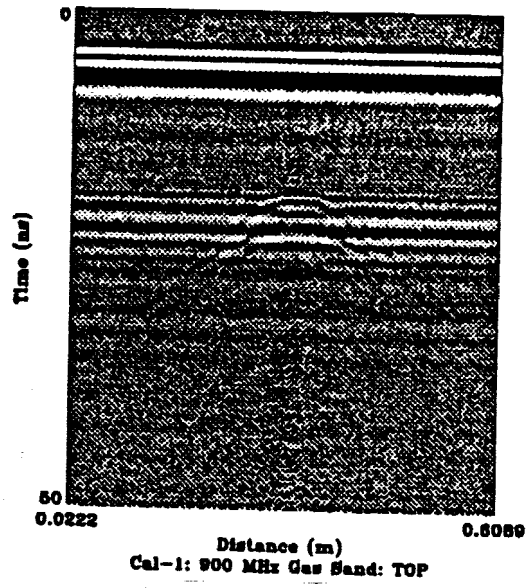

a) top calibration of 900Mhz antenna for gas & sand

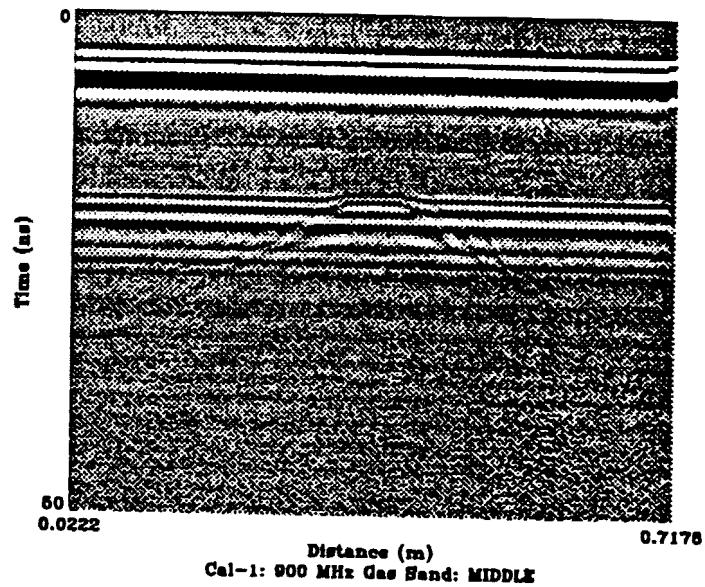

b) middle calibration of 900Mhz antenna for gas & sand

c) bottom calibration of 900Mhz antenna for gas & sand

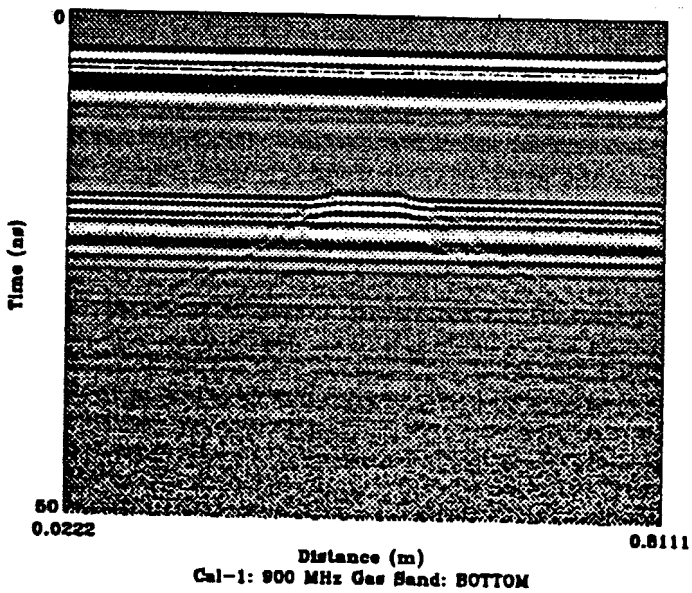

Figure 23.

File Name	cal900g1.parm Top
DC Offset	31000
Range (ns)	50
Upper Amplitude Cutoff	166
Lower Amplitude Cutoff	90
Top Sample Displayed	0
Bottom Sample Displayed	1023
Number Of Samples/Trace	1024
Two-Way Time (ns)	14.229
Velocity (m/s)	1.28*10 8
Dielectric Permittivity	5.44

a) top parameters of 900Mhz antenna for gas & sand

File Name	cal900g1.parm Middle
DC Offset	31000
Range (ns)	50
Upper Amplitude Cutoff	166
Lower Amplitude Cutoff	90
Top Sample Displayed	0
Bottom Sample Displayed	1023
Number Of Samples/Trace	1024
Two-Way Time (ns)	14.313
Velocity (m/s)	1.27*10 8
Dielectric Permittivity	5.51

b) middle parameters of 900Mhz antenna for gas & sand

File Name	cal900g1.parm Bottom
DC Offset	31000
Range (ns)	50
Upper Amplitude Cutoff	166
Lower Amplitude Cutoff	90
Top Sample Displayed	0
Bottom Sample Displayed	1023
Number Of Samples/Trace	1024
Two-Way Time (ns)	13.725
Velocity (m/s)	1.33*10 8
Dielectric Permittivity	5.06

c) bottom parameters of 900Mhz antenna for gas & sand

Table 11.

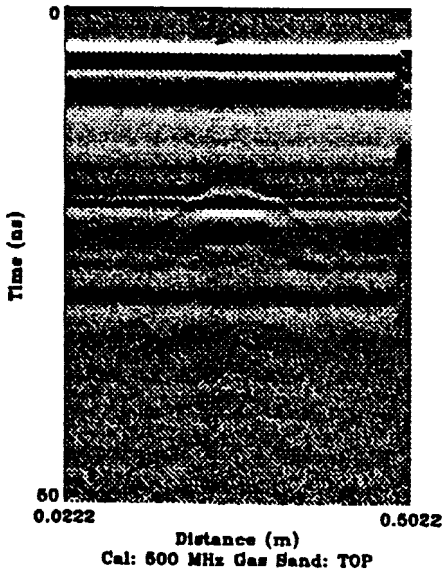

a) top calibration of 500Mhz antenna for gas & sand

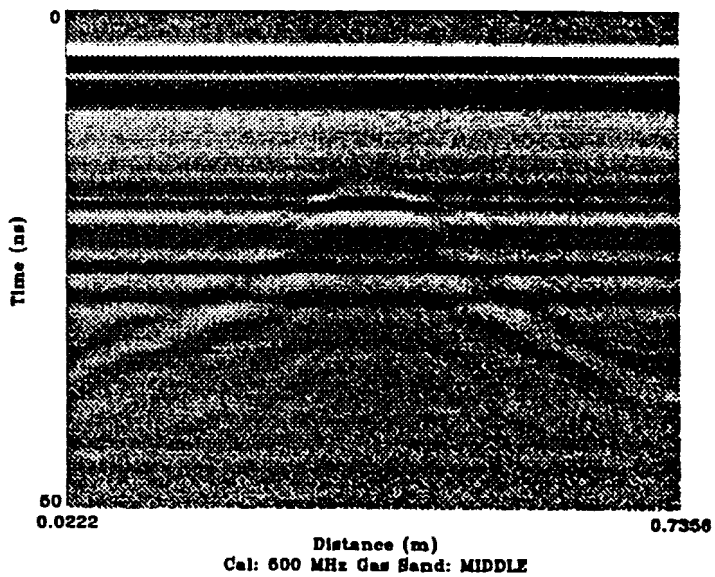

b) middle calibration of 500Mhz antenna for gas & sand

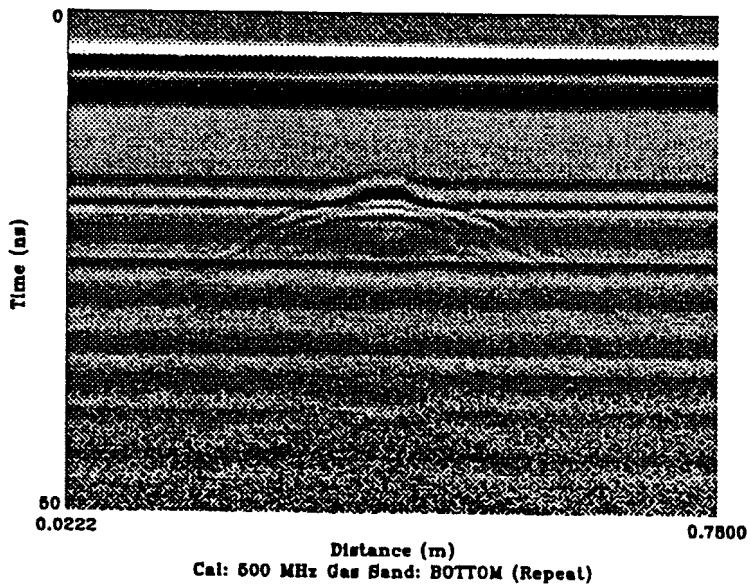

c) bottom calibration of 500Mhz antenna for gas & sand

Figure 24.

File Name	cal500g.parm Top
DC Offset	32767
Range (ns)	50
Upper Amplitude Cutoff	196
Lower Amplitude Cutoff	60
Top Sample Displayed	0
Bottom Sample Displayed	1023
Number Of Samples/Trace	1024
Two-Way Time (ns)	13.72
Velocity (m/s)	1.333*10 8
Dielectric Permittivity	5.06

a) top parameters of 500Mhz antenna for gas & sand

File Name	cal500g.parm Middle
DC Offset	32767
Range (ns)	50
Upper Amplitude Cutoff	196
Lower Amplitude Cutoff	60
Top Sample Displayed	0
Bottom Sample Displayed	1023
Number Of Samples/Trace	1024
Two-Way Time (ns)	13.529
Velocity (m/s)	1.351*10 8
Dielectric Permittivity	4.93

b) middle parameters of 500Mhz antenna for gas & sand

File Name	cal500g1.parm Bottom (Repeat)
DC Offset	32767
Range (ns)	50
Upper Amplitude Cutoff	196
Lower Amplitude Cutoff	60
Top Sample Displayed	0
Bottom Sample Displayed	1023
Number Of Samples/Trace	1024
Two-Way Time (ns)	12.795
Velocity (m/s)	1.429*10 8
Dielectric Permittivity	4.40

c) bottom parameters of 500Mhz antenna for gas & sand

Table 12.

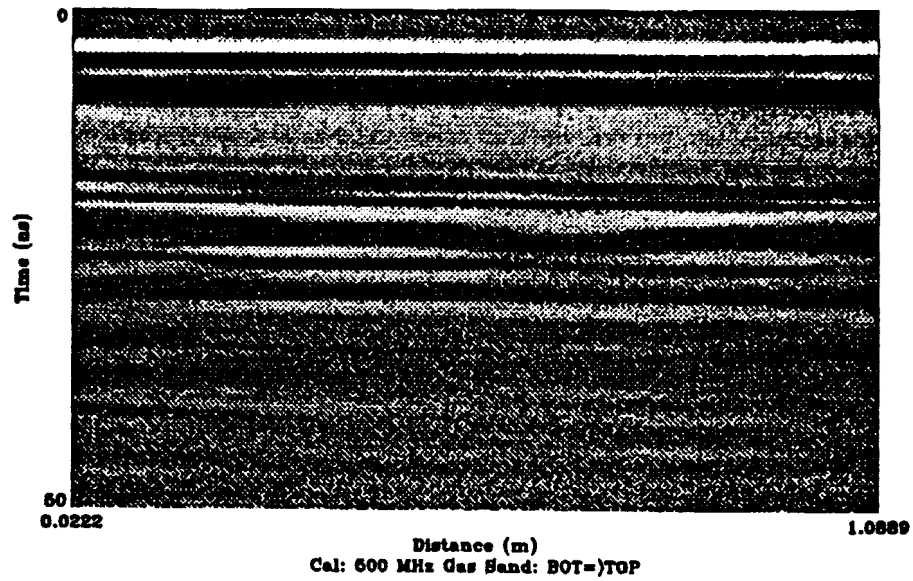
0
Time (ns)
50
0.0222
1.0889
Distance (m)
Cal: 600 MHz Gas Sand: BOT=)TOP

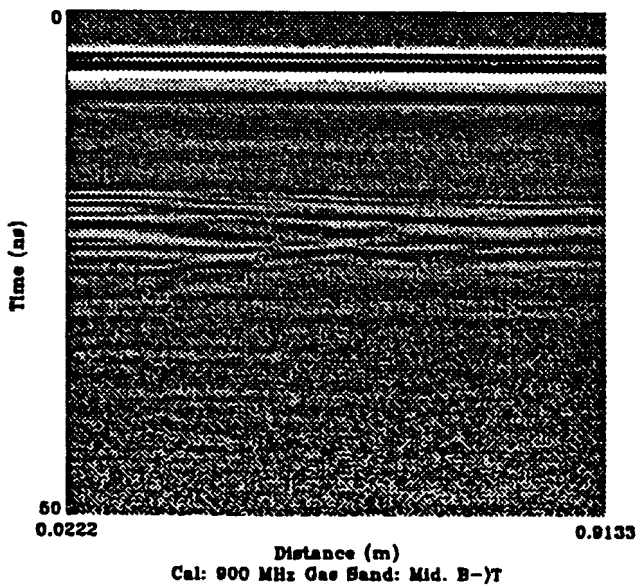
0
Time (ns)
50
0.0222
0.9133
Distance (m)
Cal: 900 MHz Gas Sand: Mid. B-)T

Figure 25.

to the top. Dielectric permittivities changed from 6.08 at the top to 19.07 at the bottom of the tank (Table 13). It should also be noted that the velocities, thus the dielectric permittivities are different between the 500Mhz and 900Mhz antennas as was the case in the other data sets. As before, a true sense of the change in velocity and permittivity can be seen in the traces that move from the bottom of the tank to the top (Figures 26-d and 27-d). Unlike Figure 25, the antennas in Figures 26-d and 27-d move from bottom to top, as the records move from right to left. The sloping reflection, as found in Figure 25, is even more prominent with the presence of water (see Figures 26-d and 27-d). The 500Mhz antenna is especially interesting, as there seems to be an increase in the reflection time located in the middle of Figure 26-d. This increase appears as a small hump in the middle of the record. The feature is most likely due to the small amount of gas floating on the surface of the water. All of the above parameters are located in Tables 13 and 14. It should be noted there are some changes in the velocities and dielectric permittivities in the top and middle of the tank. The velocities of the signal in these areas increases during the duration of the experiment. This is no doubt due to the fact that gasoline vapors are not only moving through but also accumulating in the unsaturated zone.

The last set of calibrations to be observed will be the second set of slug records taken after the tank system was left to equalize overnight. The parameters for this set are located in Tables 15-16 and Figures 28-29. The differences in recording abilities of the 500Mhz and 900Mhz antennas are very prominent in

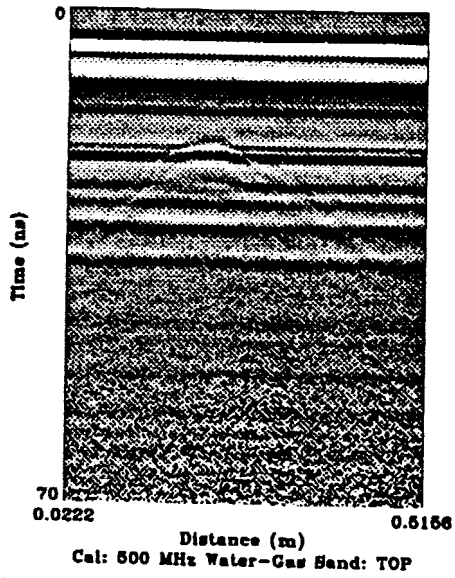

a) top calibration of 500Mhz antenna for water-gas-sand

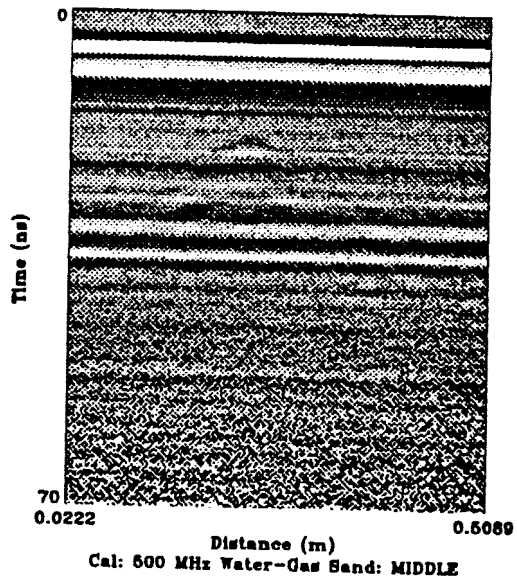

b) middle calibration of 500Mhz antenna for water-gas-sand

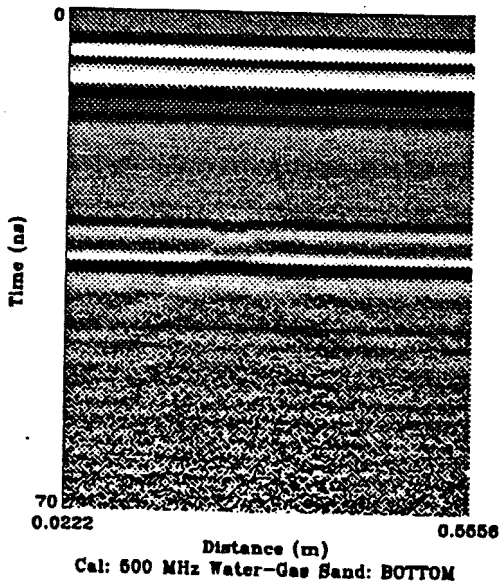

c) bottom calibration of 500Mhz antenna for water-gas-sand

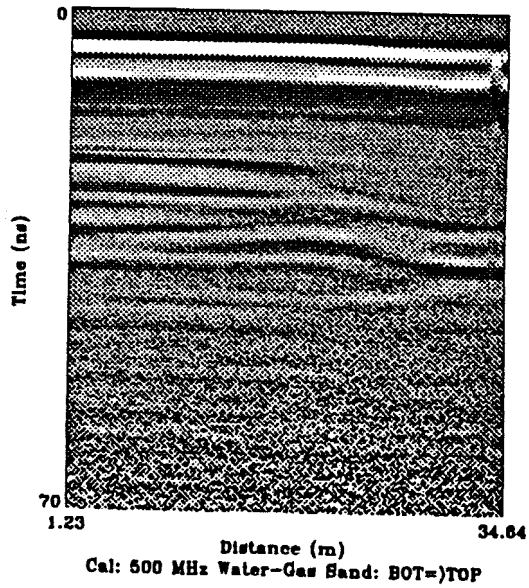

d) 500Mhz scan from bottom to top (right to left) for water-gas-sand

Figure 26.

File Name	cal500w.parm Top
DC Offset	31000
Range (ns)	70
Upper Amplitude Cutoff	166
Lower Amplitude Cutoff	90
Top Sample Displayed	0
Bottom Sample Displayed	1023
Number Of Samples/Trace	1024
Two-Way Time (ns)	15.039
Velocity (m/s)	1.216*10 8
Dielectric Permittivity	6.08

a) top parameters of 500Mhz antenna for water-gas-sand

File Name	cal500w.parm Middle
DC Offset	31000
Range (ns)	70
Upper Amplitude Cutoff	166
Lower Amplitude Cutoff	90
Top Sample Displayed	0
Bottom Sample Displayed	1023
Number Of Samples/Trace	1024
Two-Way Time (ns)	15.098
Velocity (m/s)	1.211*10 8
Dielectric Permittivity	6.13

b) middle parameters of 500Mhz antenna for water-gas-sand

File Name	cal500w.parm Bottom
DC Offset	32000
Range (ns)	70
Upper Amplitude Cutoff	156
Lower Amplitude Cutoff	100
Top Sample Displayed	0
Bottom Sample Displayed	1023
Number Of Samples/Trace	1024
Two-Way Time (ns)	26.627ns
Velocity (m/s)	6.868*10 7
Dielectric Permittivity	19.07

c) bottom parameters of 500Mhz antenna for water-gas-sand

File Name	cal500w.parm Bot=>Top
DC Offset	31000
Range (ns)	70
Upper Amplitude Cutoff	176
Lower Amplitude Cutoff	80
Top Sample Displayed	0
Bottom Sample Displayed	1023
Number Of Samples/Trace	1024
Two-Way Time (ns)	
Velocity (m/s)	
Dielectric Permittivity	

d) 500Mhz scan from bottom to top (right to left) for water-gas-sand

Table 13.

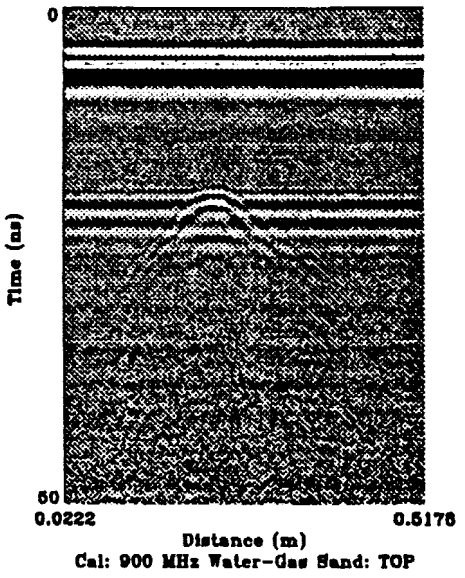

a) top calibration of 900Mhz antenna for water-gas-sand

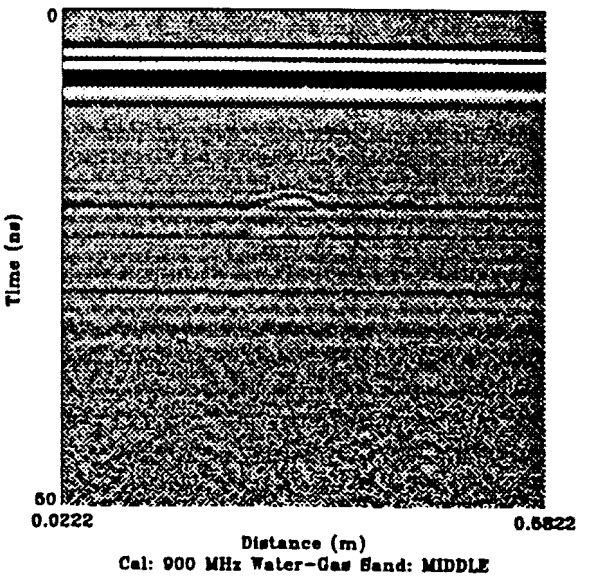

b) middle calibration of 900Mhz antenna for water-gas-sand

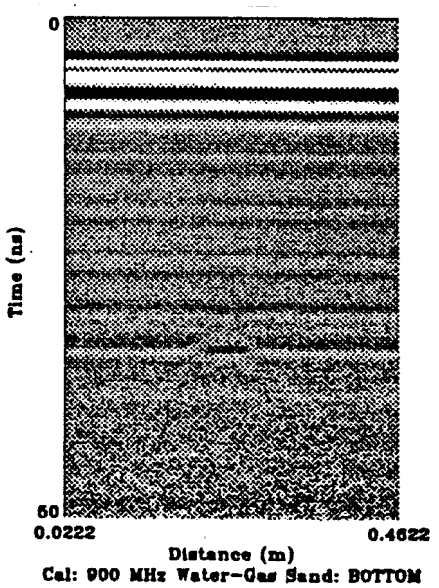

c) bottom calibration of 900Mhz antenna for water-gas-sand

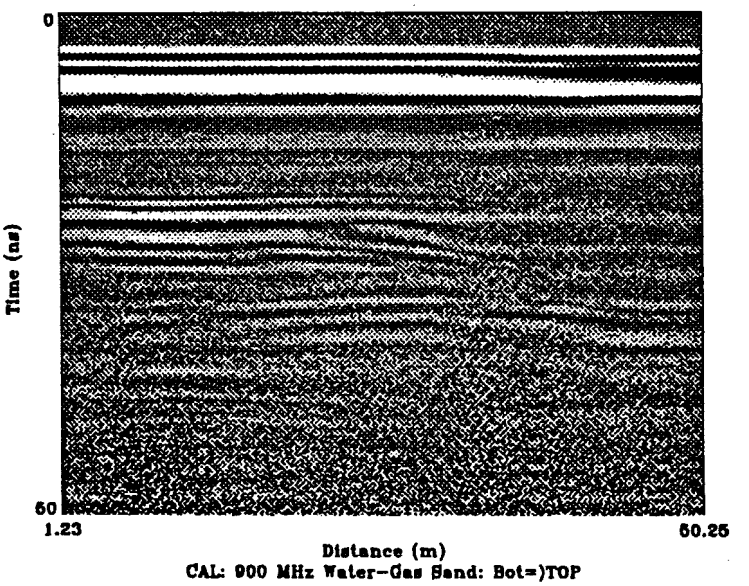

d) 900Mhz scan from bottom to top (right to left) for water-gas-sand

Figure 27.

File Name	cal900w.parm Top
DC Offset	31000
Range (ns)	50
Upper Amplitude Cutoff	176
Lower Amplitude Cutoff	80
Top Sample Displayed	0
Bottom Sample Displayed	1023
Number Of Samples/Trace	1024
Two-Way Time (ns)	14.705
Velocity (m/s)	1.243*10 8
Dielectric Permittivity	5.81

a) top parameters of 900Mhz antenna for water-gas-sand

File Name	cal900w.parm Middle
DC Offset	31000
Range (ns)	50
Upper Amplitude Cutoff	176
Lower Amplitude Cutoff	80
Top Sample Displayed	0
Bottom Sample Displayed	1023
Number Of Samples/Trace	1024
Two-Way Time (ns)	14.313
Velocity (m/s)	1.277*10 8
Dielectric Permittivity	5.51

b) middle parameters of 900Mhz antenna for water-gas-sand

File Name	cal900w.parm Bottom
DC Offset	31000
Range (ns)	50
Upper Amplitude Cutoff	156
Lower Amplitude Cutoff	100
Top Sample Displayed	0
Bottom Sample Displayed	1023
Number Of Samples/Trace	1024
Two-Way Time (ns)	25.490
Velocity (m/s)	7.175*10 7
Dielectric Permittivity	17.48

c) bottom parameters of 900Mhz antenna for water-gas-sand

File Name	cal900w.parm Bot=>Top
DC Offset	32767
Range (ns)	50
Upper Amplitude Cutoff	156
Lower Amplitude Cutoff	100
Top Sample Displayed	0
Bottom Sample Displayed	1023
Number Of Samples/Trace	1024
Two-Way Time (ns)	
Velocity (m/s)	
Dielectric Permittivity	

d) parameters of 900Mhz antenna for bottom to top (right to left)

Table 14.

this data set. For example, the contrasts in dielectric permittivities for the two antennas. The 500Mhz antenna reveals dielectrics from 3.97 at the top of the tank to 7.47 in the bottom (Table 16). The 900Mhz antenna yields dielectric permittivities from 7.45 at the top of the tank to 17.21 at the bottom (Table 15). It also should be noted, the changes in velocity and dielectric permittivity in the upper portions of the tank are no longer present, as was found in the gas and water-gas data sets. This due to the placement of water into the tank system from the top down. Thus, with the presence of water throughout the system and displacement of gasoline vapors in the unsaturated zone, dielectric permittivities are increased and wave velocities are decreased. The decrease in wave velocity (i.e., reflection times) is very prominent in Figures 28-d and 29-d. These GPR records, like the ones in Figures 26-d and 27-d, move from the bottom of the tank to the top (from right to left). The resulting reflection appears to be dipping stratigraphic beds, but is actually caused by the decrease in wave velocities as the water saturation increases. Note: With the increasing presence of water the signal strength decreased.

Two-Dimensional Figures

Three two-dimensional GPR records can be found in Figures 30-32. These records are all taken from the side scans of the 900Mhz antenna. These scans include: dry sand, gas and sand, and water, gas, and sand. Note: trace 04 is near the top of the tank and trace 10 is near the bottom of the tank. Figure 36 contains a color scale for the GPR signal amplitude.

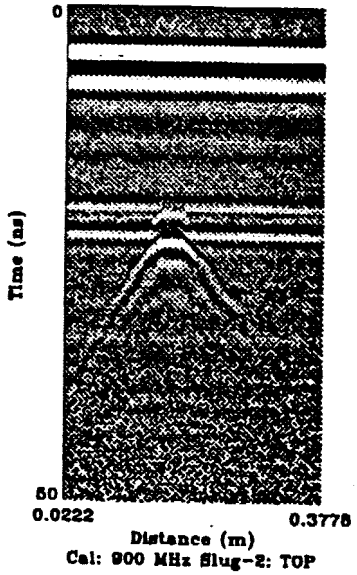

a) top calibration of 900Mhz antenna for slug

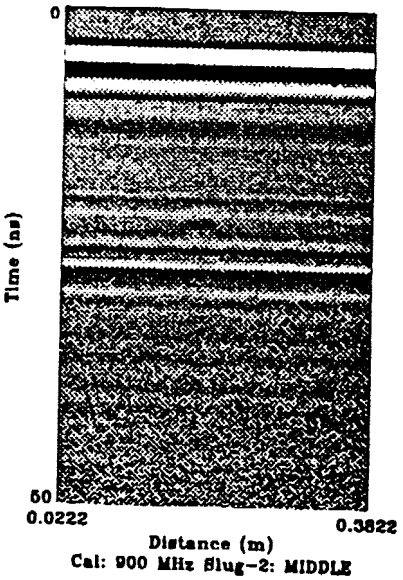

b) middle calibration of 900Mhz antenna for slug

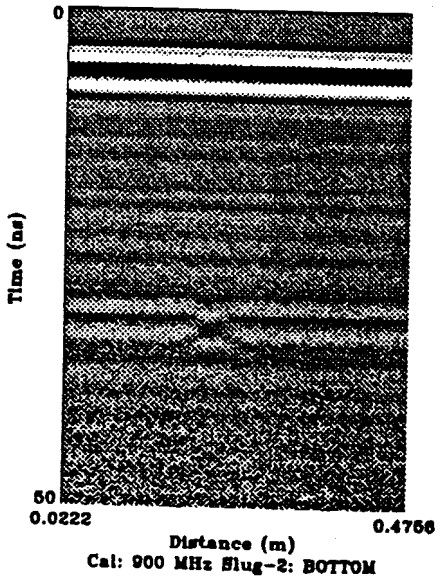

c) bottom calibration of 900Mhz antenna for slug

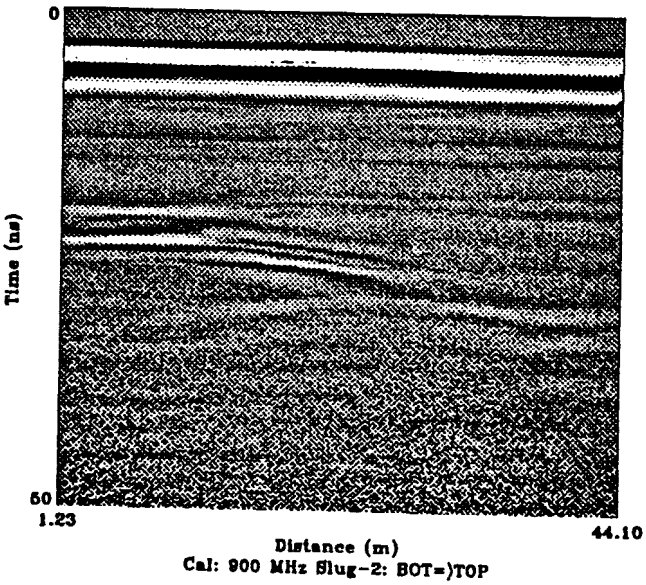

d) 900Mhz scan from bottom to top (right to left) for slug

Figure 28.

File Name	cal900s2.parm Top
DC Offset	32000
Range (ns)	50
Upper Amplitude Cutoff	156
Lower Amplitude Cutoff	100
Top Sample Displayed	0
Bottom Sample Displayed	1023
Number Of Samples/Trace	1024
Two-Way Time (ns)	16.666
Velocity (m/s)	1.097*10 8
Dielectric Permittivity	7.47

a) top parameters of 900Mhz antenna for slug

File Name	cal900s2.parm Middle
DC Offset	32000
Range (ns)	50
Upper Amplitude Cutoff	156
Lower Amplitude Cutoff	100
Top Sample Displayed	0
Bottom Sample Displayed	1023
Number Of Samples/Trace	1024
Two-Way Time (ns)	16.666
Velocity (m/s)	1.097*10 8
Dielectric Permittivity	7.47

b) middle parameters of 900Mhz antenna for slug

File Name	cal900s2.parm Bottom
DC Offset	32000
Range (ns)	50
Upper Amplitude Cutoff	156
Lower Amplitude Cutoff	100
Top Sample Displayed	0
Bottom Sample Displayed	1023
Number Of Samples/Trace	1024
Two-Way Time (ns)	25.294
Velocity (m/s)	7.230*10 7
Dielectric Permittivity	17.21

c) bottom parameters of 900Mhz antenna for slug

File Name	cal900s2.parm Bot=>Top
DC Offset	32000
Range (ns)	50
Upper Amplitude Cutoff	156
Lower Amplitude Cutoff	100
Top Sample Displayed	0
Bottom Sample Displayed	1023
Number Of Samples/Trace	1024
Two-Way Time (ns)	
Velocity (m/s)	
Dielectric Permittivity	

d) 900Mhz scan parameters from bottom to top (right to left) for slug

Table 15.

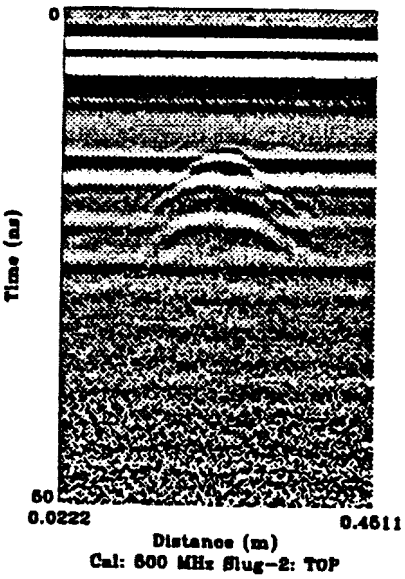

a) top calibration of 500Mhz antenna for slug

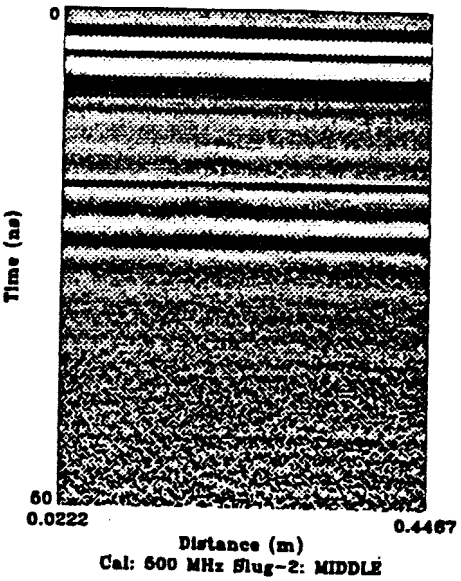

b) middle calibration of 500Mhz antenna for slug

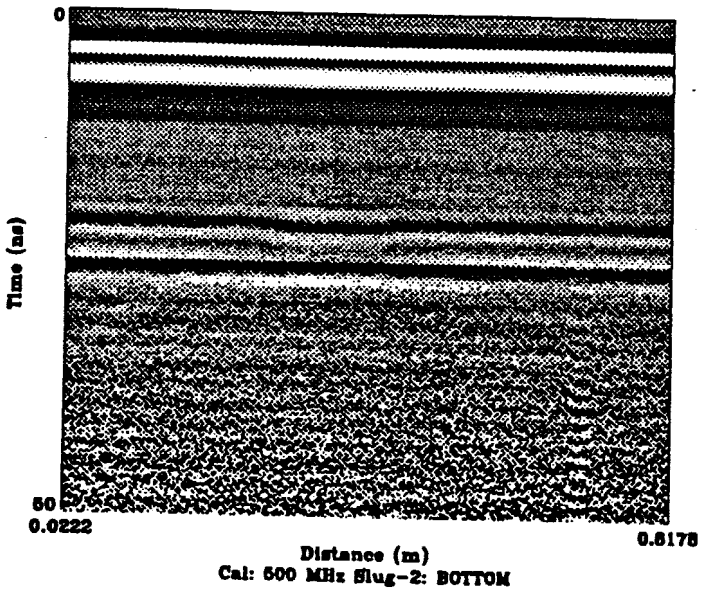

c) bottom calibration of 500Mhz antenna for slug

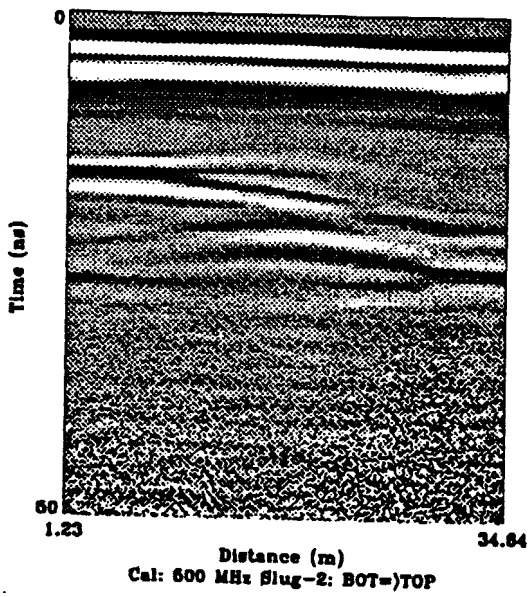

d) 500Mhz scan from bottom to top (right to left) for slug

Figure 29.

File Name	cal500s2.parm Top
DC Offset	31000
Range (ns)	50
Upper Amplitude Cutoff	156
Lower Amplitude Cutoff	100
Top Sample Displayed	0
Bottom Sample Displayed	1023
Number Of Samples/Trace	1024
Two-Way Time (ns)	12.156
Velocity (m/s)	1.504*10 8
Dielectric Permittivity	3.97

a) top parameters of 500Mhz antenna for slug

File Name	cal500s2.parm Middle
DC Offset	31000
Range (ns)	50
Upper Amplitude Cutoff	166
Lower Amplitude Cutoff	90
Top Sample Displayed	0
Bottom Sample Displayed	1023
Number Of Samples/Trace	1024
Two-Way Time (ns)	11.568
Velocity (m/s)	1.581*10 8
Dielectric Permittivity	3.60

b) middle parameters of 500Mhz antenna for slug

File Name	cal500s2.parm Bottom
DC Offset	31000
Range (ns)	50
Upper Amplitude Cutoff	156
Lower Amplitude Cutoff	100
Top Sample Displayed	0
Bottom Sample Displayed	1023
Number Of Samples/Trace	1024
Two-Way Time (ns)	16.666
Velocity (m/s)	1.097*10 8
Dielectric Permittivity	7.47

c) bottom parameters of 500Mhz antenna for slug

File Name	cal500s2.parm Bot=>Top
DC Offset	31000
Range (ns)	50
Upper Amplitude Cutoff	156
Lower Amplitude Cutoff	100
Top Sample Displayed	0
Bottom Sample Displayed	1023
Number Of Samples/Trace	1024
Two-Way Time (ns)	
Velocity (m/s)	
Dielectric Permittivity	

d) 500Mhz scan parameters from bottom to top (right to left) for slug

Table 16.

Figure 30 displays two GPR records from the dry sand portion of the tank experiment. Note: these records are from the viewpoint of looking directly down onto the top of the tank. Some notable features of these records are the reflections from the walls of the tank, high frequency noise, and the reflection from the back side of the tank. Note the loss of negative amplitude in the bottom of Figure 30-b, when compared to Figure 30-a.

Figure 31 contains two records from the gas and sand part of the experiment. These two records are essentially the same as what was found in Figure 30. Some noticeable differences are the loss of negative amplitude not only between Figures 31-a and 31-b, but also between both, Figures 31a & b and Figures 30a & b. There is also loss of high frequency noise. Neither trace is moving directly through the gas saturated zone. Although we know from the calibration lines, velocities are increased due to the presence of gasoline vapors.

Figure 32 shows two records from the water, gas, and sand fraction of the experiment. There appears to be loss of the high frequency noise but this may be due in part from the fact that the total record length (50ns) has been displayed. The amplitude differences between Figures 32a & b are the most distinct of all the GPR records. This is interpreted to be caused by the presence of water saturation within trace 17, thus the slowing of wave velocities. There are no truly distinctive changes in the records, but from the calibration, we know the velocity in the bottom of the tank has been decreased due to the water and the velocity in the top has been increased due to the gas vapor.

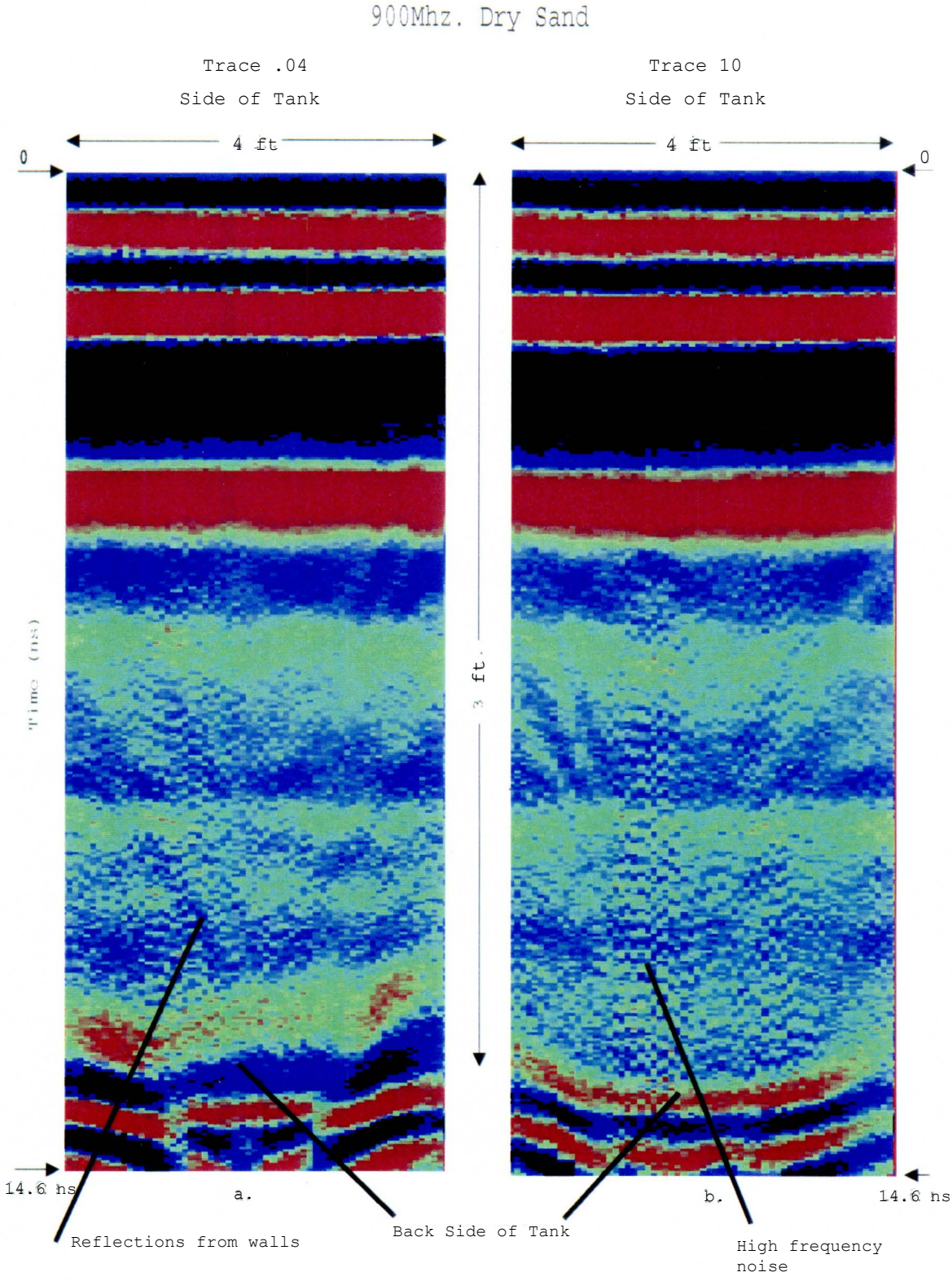

Figure 30. Two-dimensional GPR records from the 900mhz antenna for dry sand.

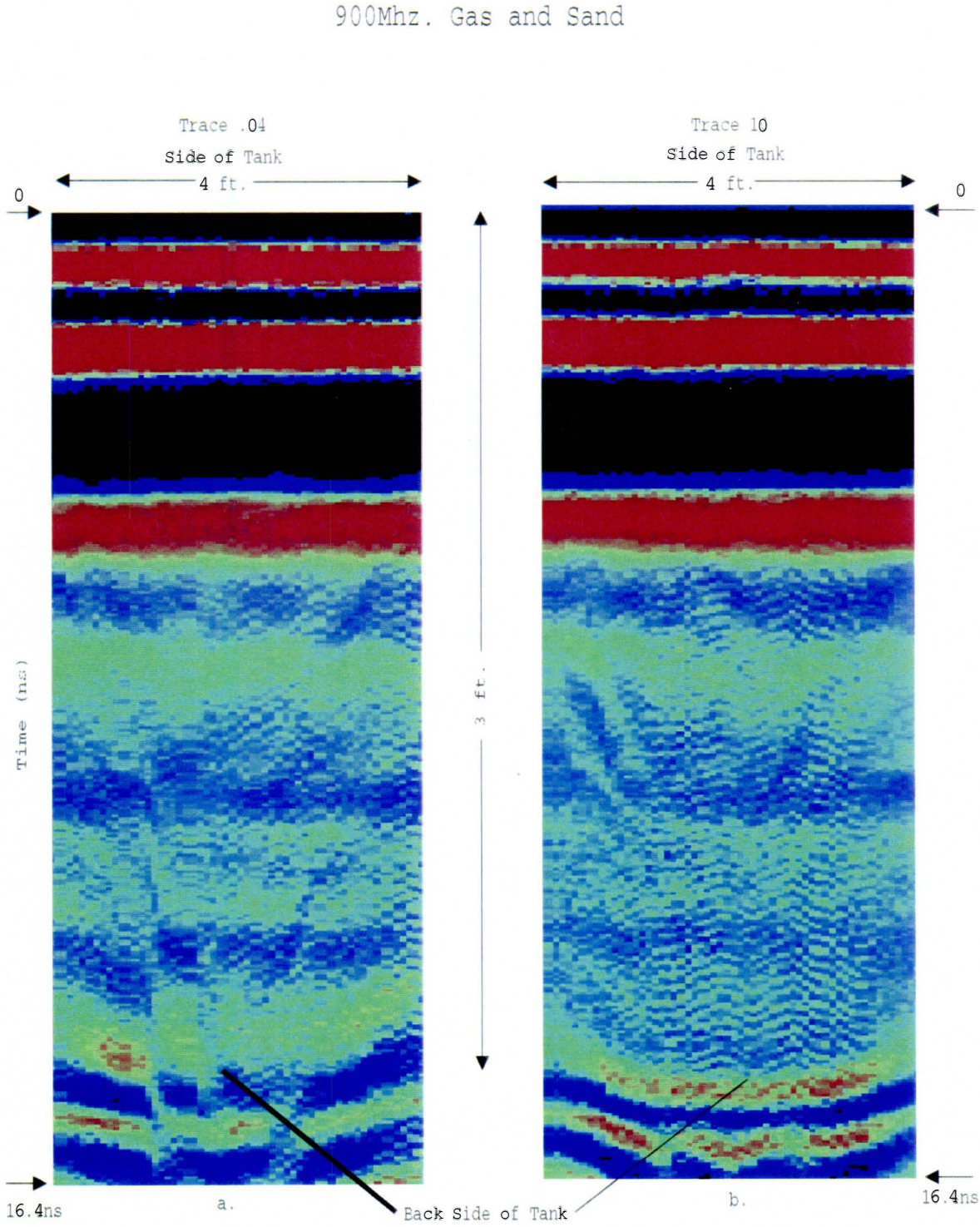

Figure 31. Two-dimensional GPR records from the 900Mhz antenna for gas and sand.

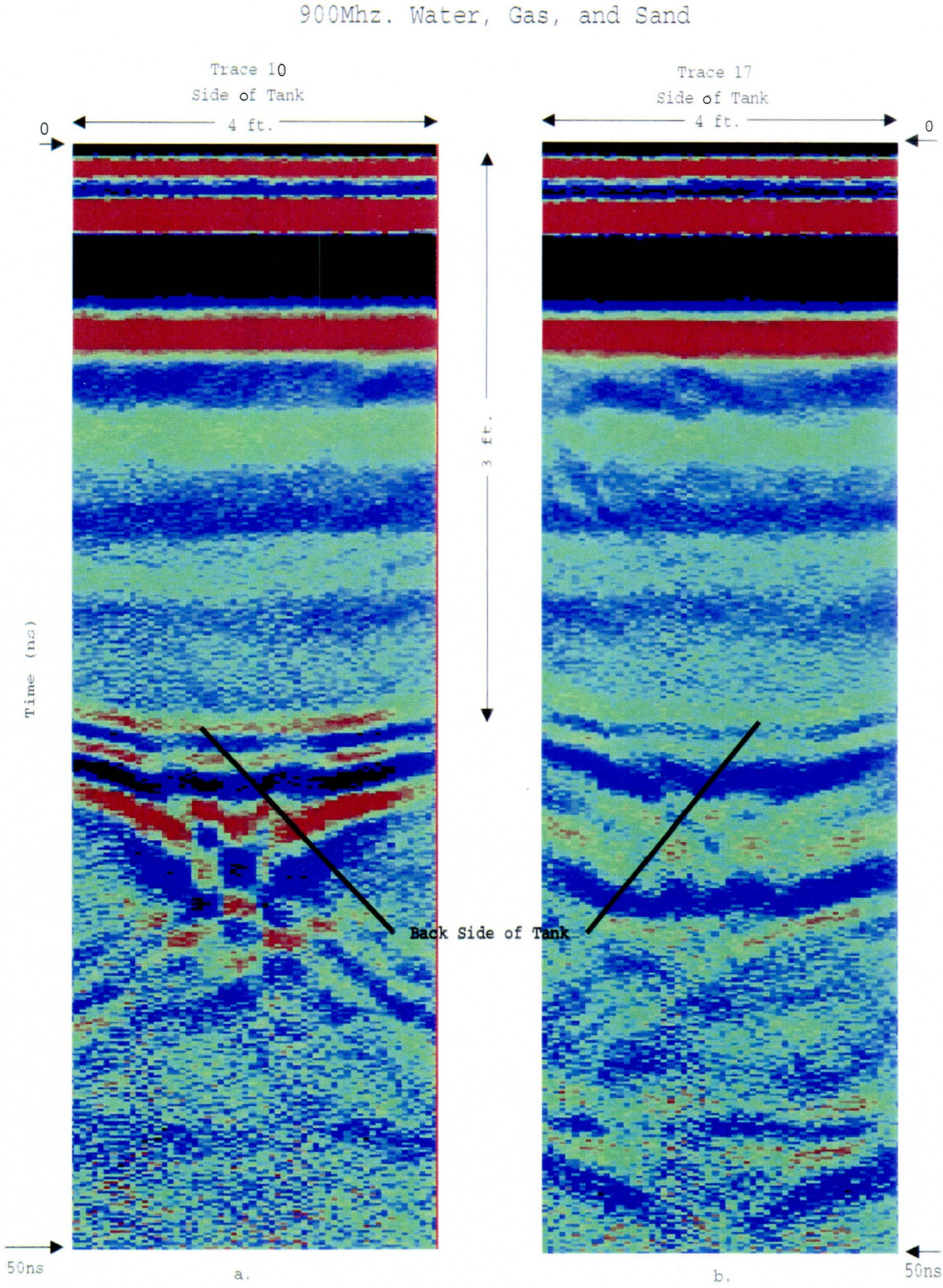

Figure 32. Two-dimensional GPR records from the 900Mhz antenna for water, gas, and sand.

Three-Dimensional GPR

The same three series of data sets are used for the 3-D images: dry sand, gas and sand, and water, gas, and sand. These 3-D images are created by placing all of the individual records together into one 3-D image. These images can be found in Figures 33-35. The point of view for these images is looking directly at one of the sides of the tank. As stated before, a color scale for the GPR signal amplitude is located in Figure 36. Figure 33 contains the 3-D display for the dry sand part of the experiment. The important features to notice are the signal loss out the top of the tank, and the reflection from the back of the tank. If the tank was to be sealed at the top by acrylic (of equal thickness as the rest) the received signal would be similar to what is recorded in the bottom of the tank. Also note, the fact that since the medium of the tank is perfectly homogenous, no reflections are present.

Figure 34 shows the 3-D image for the sand and gas portion of the experiment. We see that signal loss out of the top of the tank seems to be reduced. This is most likely the result of the increase in wave velocity due to the presence of gasoline vapors in the unsaturated zone. Also, as we know from the calibration, there is a signal increase from the gasoline saturation in the bottom of the tank. This can be interpreted from the image by the loss of noise in the bottom of the tank.

Figure 35 consists of the 3-D record from the water, gas, and sand part of the experiment. If Figure 35 is compared with Figure 34, a noticeable difference can be seen in the bottom reflections

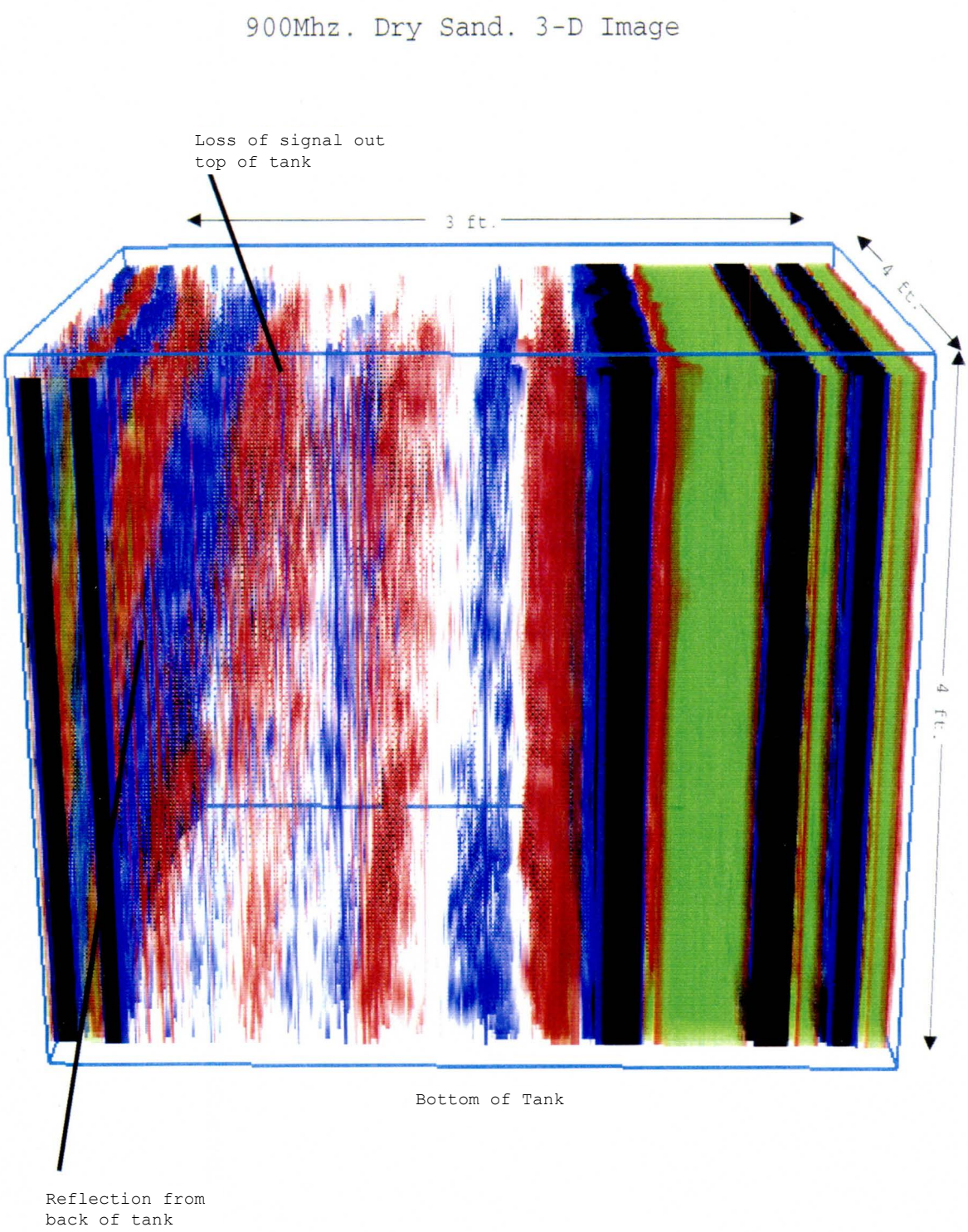

Figure 33. Three-dimensional GPR record from the 900Mhz antenna for dry sand.

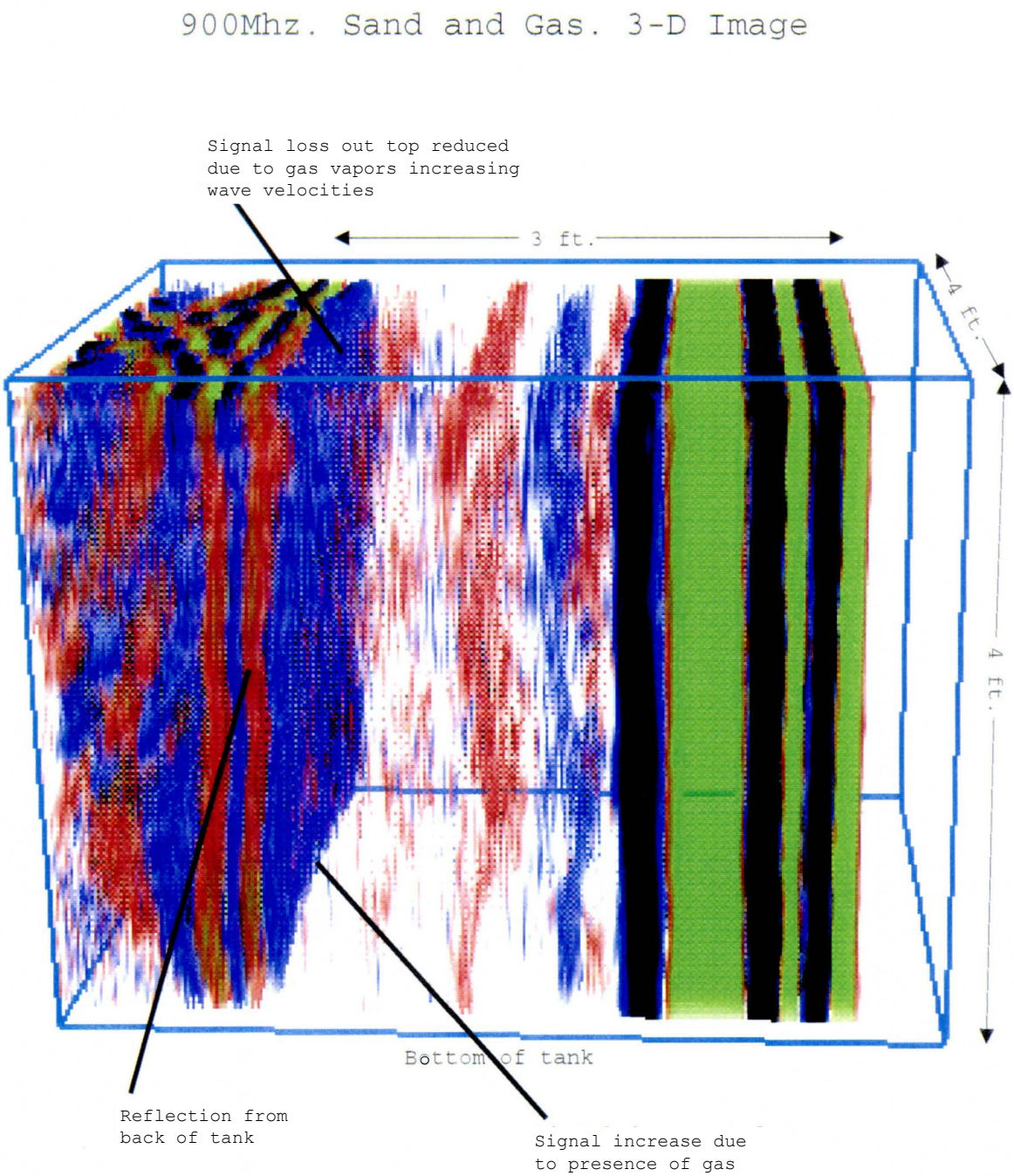

Figure 34. Three-dimensional GPR record form the 900Mhz antenna for sand and gas.

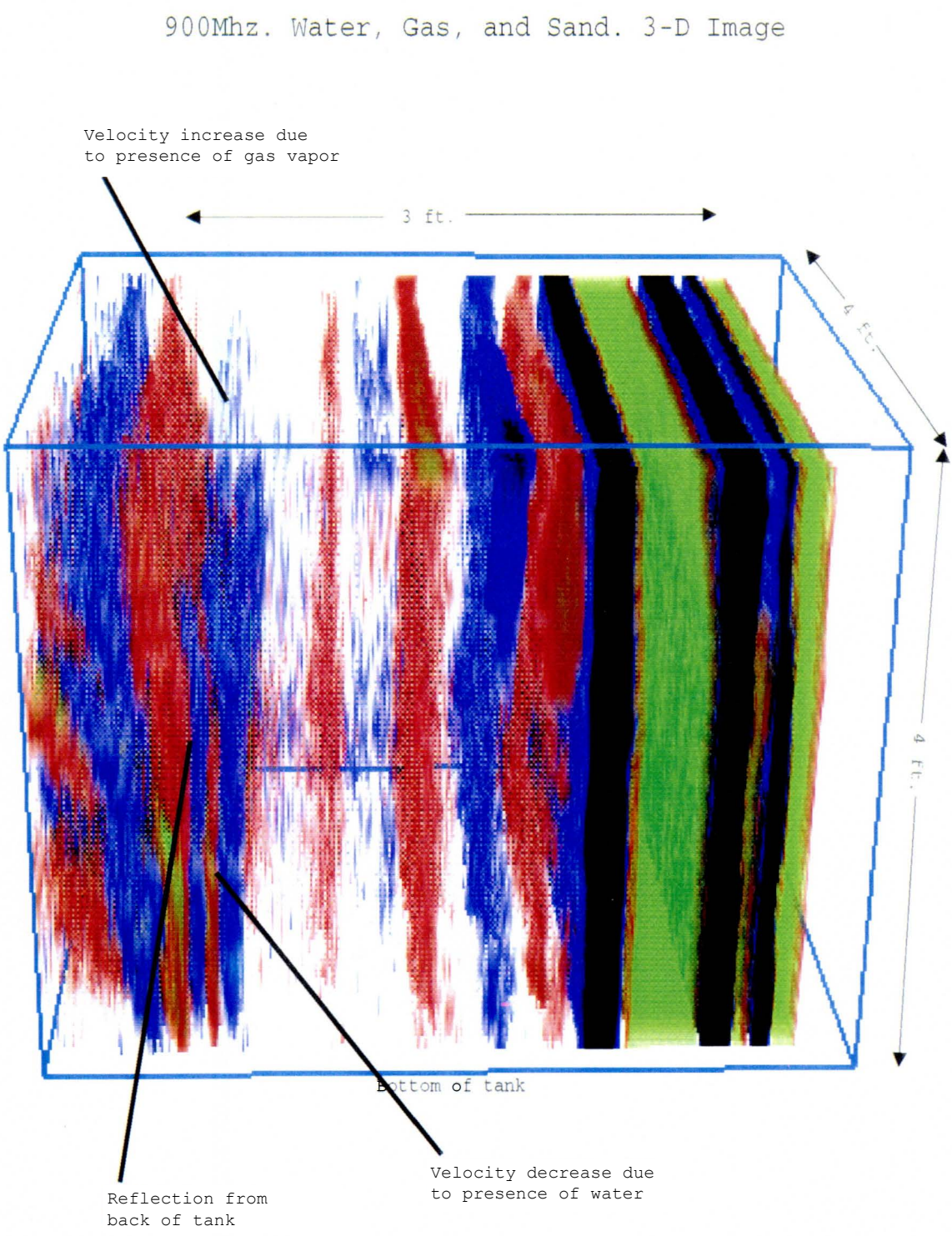

Figure 35. Three-dimensional record from the 900Mhz antenna for water, gas, and sand.

Figure 36. Color Scale for GPR Signal Amplitude

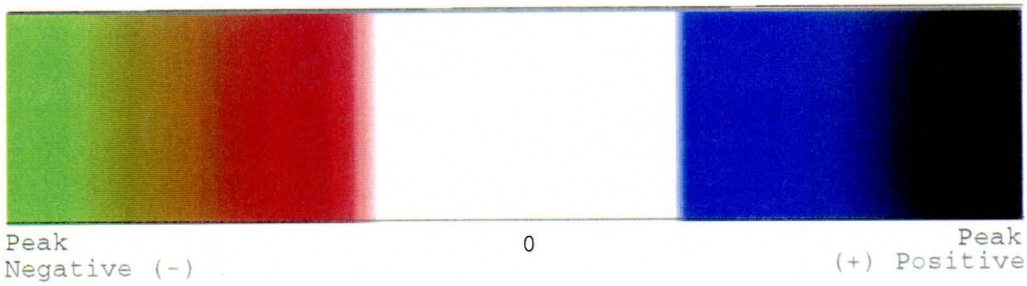

of the two Figures. There is a definite decrease in wave velocity in the bottom of Figure 35 due to the presence of water saturation. As with Figure 34, there is a known increase in wave velocity (from calibrations) in the upper section of the image. This is illustrated as a sloping of the reflection in the top section of the 3-D image. It should also be noted that within the bottom portion of the reflection from the back of the tank there is a peak negative amplitude. This is interpreted as the presence of the gasoline saturation zone upon the water table within the tank.

To conclude, the GPR system did not readily detect (i.e., produce a definite reflection in all cases) the presence of a small amount (15 gallons) of gasoline or gasoline vapor. It was detectable in the fact that: wave velocities were increased on the order of 5.00×10^6 m/s, there was a reduction of permittivities, and there was the presence of a peak negative amplitude within the 3-D water, gas, and sand image. Top and side records of the tank showed no "significant" reflections from the gasoline zones. Although, the arrival time of the bottom and back-side reflections did change, as illustrated in the calibrations.

With the addition of water, wave velocities were reduced on the order of 5.73×10^7 m/s. Thus, reflection arrival times for the back-side of the tank were reduced, as illustrated in the calibrations. It was also noted that the dielectric permittivities increased with the presence of water. No significant reflections were produced in the top or side scans from any of the water zones (i.e., water saturation or capillary fringe). As stated before, only reflection arrival times changed.

The described experiment is currently being continued by Dr. Jeffrey J. Daniels, Professor at The Ohio State University and Mr. David Grumman, a Masters student in geophysics at The Ohio State University. The experiment will be expanded (following the above guidelines), to include the addition of diesel fuel in sand. It will also be repeated in order to replace the sand medium with a sand-clay mixture.

References

Annan, A.P., Bauman, P., Greenhouse, J.P., and Redman, J.D., 1991, Geophysics and DNAPLS: Proceedings of the 1991 Outdoor Action Conference, Las Vegas, NV. pp. 963-977

Beres Jr, M., and Haeni, F.P., 1991, Application of Ground-Penetrating-Radar Methods in Hydrogeologic Studies: Ground Water, May-June, 1991. Vol. 29, No. 3. pp. 375-386

Bruell, C.J., and Hoag, G.E., 1986, The Diffusion of Gasoline-Range Hydrocarbon Vapors in Porous Media, Expermental Methodologies: Proceedings of the NWWA Conference on Petroleum Hydrocarbons and Organic Chemicals in Ground Water. Prevention, Detection, and Restoration, November 12-14, 1986. Houston, TX. pp. 420-443

Daniels, J.J., 1989, Fundamentals of Ground Penetrating Radar: Proceedings of the Symposium on the Application of Geophysics to Engineering and Environmental Problems, March 13-16, 1989. Society of Mining and Engineering Geophysicists, Denver, CO.

Daniels, J.J., Roberts, R., 1994. Ground Penetrating Radar for Geotechnical Applications; in Geophysical Characterization of Sites: American Society of Civil Engineers ISSMFE #10 Publication on Geophysics, special volume XIII ICSMFE, 1994, New Delhi, India, p. 1-13.

Dietz, D.N., Pollution of Permeable Strata by Oil Components, 1967? (Unknown Reference).

Lyman, W.J., Reidy, P.J., and Levy, B., 1992, Mobility and

Degradation of Organic Contaminants in Subsurface Environments: C.K. Smoley, Inc. Chelsea, Michigan, 356p.

Olhoeft, G.R., 1986, Direct Detection of Hydrocarbon and Organic Chemicals with Ground Penetrating Radar and Complex Resistivity: Proceedings of the NWWA Conference on Petroleum Hydrocarbons and Organic Chemicals in Ground Water. Prevention, Detection, and Restoration, November 12-14, 1986. Houston, TX. pp. 1-22

Redman, J.D., Kueper, B.H., and Annan, A.P., 1991, Dielectric Stratigraphy of a DNAPL Spill and Implications for Detection with Ground Penetrating Radar: Proceedings of the 1991 Outdoor Action Conference, Las Vegas, NV. pp. 1017-1030

Schwille, F., Petroleum Contaminantion of the Subsoil-A Hydrological Problem: The Joint Problems of the Oil and Water Industries, Institute of Peteroleum, London, 1967. pp.23-54

Walther, E.G., Pitchford, A.M., and Olhoeft, G.R., A Strategy for Detecting Subsurface Organic Contaminants: Proceedings of the NWWA Conference on Peteroleum Hydrocarbons and Organic Chemicals in Ground Water. Prevention, Detection, and Restoration, November 12-14, 1986. Houston, TX. pp 375-381